

ORNL

OAK RIDGE
NATIONAL
LABORATORY

MARTIN MARIETTA

OPERATED BY
MARTIN MARIETTA ENERGY SYSTEMS, INC.
FOR THE UNITED STATES
DEPARTMENT OF ENERGY

MARTIN MARIETTA ENERGY SYSTEMS LIBRARIES

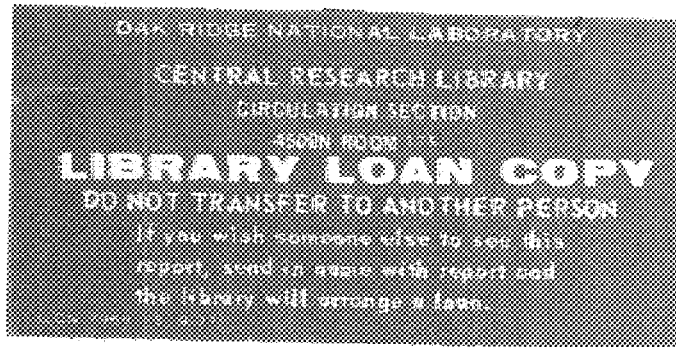


3 4456 0137921 1

ORNL/TM-9919

**Development and Evaluation of
DOTTOR, A Computer Code to Couple
Two-Dimensional to Three-Dimensional
Discrete Ordinates Calculations**

J. L. Thompson
M. B. Emmett
H. L. Dodds, Jr.



Printed in the United States of America. Available from
National Technical Information Service
U.S. Department of Commerce
5285 Port Royal Road, Springfield, Virginia 22161
NTIS price codes—Printed Copy: A05 Microfiche: A01

This report was prepared as an account of work sponsored by an agency of the United States Government. Neither the United States Government nor any agency thereof, nor any of their employees, makes any warranty, express or implied, or assumes any legal liability or responsibility for the accuracy, completeness, or usefulness of any information, apparatus, product, or process disclosed, or represents that its use would not infringe privately owned rights. Reference herein to any specific commercial product, process, or service by trade name, trademark, manufacturer, or otherwise, does not necessarily constitute or imply its endorsement, recommendation, or favoring by the United States Government or any agency thereof. The views and opinions of authors expressed herein do not necessarily state or reflect those of the United States Government or any agency thereof.

Engineering Physics & Mathematics Division

DEVELOPMENT AND EVALUATION OF DOTTOR, A
COMPUTER CODE TO COUPLE TWO-DIMENSIONAL
TO THREE-DIMENSIONAL DISCRETE
ORDINATES CALCULATIONS

J. L. Thompson*
M. B. Emmett**
H. L. Dodds, Jr.‡

*Thesis presented for Master of Science Degree at The University of Tennessee,
Knoxville, Tennessee

**Computing and Telecommunications Division

‡Nuclear Engineering Department, The University of Tennessee, Knoxville, Tennessee

Date Published - April 1986

NOTE:

This work supported by Defense Nuclear Agency
under Subtask PE074

Prepared by the
Oak Ridge National Laboratory
Oak Ridge, Tennessee 37831
operated by
Martin Marietta Energy Systems, Inc.,
for the
U.S. DEPARTMENT OF ENERGY
under Contract No. DE-AC05-84OR21400



TABLE OF CONTENTS

SECTION	PAGE
1. INTRODUCTION	1
2. METHOD DEVELOPMENT	5
2.1 POSITION DETERMINATION	5
2.2 2-D TO 3-D QUADRATURE TRANSFORMATION	9
2.3 QUADRATURE ROTATION AND REDUCTION	12
2.4 SPATIAL INTERPOLATION	19
3. METHOD IMPLEMENTATION AND EVALUATION	22
4. SUMMARY, CONCLUSIONS, AND FUTURE WORK	29
LIST OF REFERENCES	30
APPENDIXES	32
APPENDIX A CODE DESCRIPTION	33
APPENDIX B INPUT DATA DESCRIPTION	48
APPENDIX C SAMPLE PROBLEM INPUT AND OUTPUT	50
APPENDIX D DOTTOR OUTPUT FILE FORMAT	69
APPENDIX E VISTA CODE DESCRIPTION	76

LIST OF FIGURES

FIGURE	PAGE
1. Problem geometry	2
2. Computer code relationships and functions	4
3. Angle α varies for points on different radial vectors	7
4. Position of the 2-D Z-axis (X_D, Y_D), in the 3-D X-Y plane for (a) $0 \leq \alpha \leq \frac{\pi}{2}$, (b) $\frac{\pi}{2} < \alpha \leq \pi$, (c) $\pi < \alpha \leq \frac{3\pi}{2}$, and (d) $\frac{3\pi}{2} < \alpha \leq 2\pi$	8
5. Representation of (a) a 2-D quadrature, and (b) a 3-D quadrature	11
6. Solid angle boundaries	13
7. Eta levels in a level symmetric quadrature	16
8. Quadrature reduction and rotation	18
9. Spatial interpolation	20
10. Comparison of (a) original and (b) modified DOTTOR algorithms	25
A.1. Computer codes used and their I/O files	34
C.1. DOTTOR sample problem input	51
C.2. DOTTOR sample problem output	52

LIST OF TABLES

TABLE		PAGE
1.	Comparison of Group 1 DOT Scalar Fluxes with TORT Scalar Fluxes Using the Original DOTTOR Algorithm	24
2.	Comparison of Group 2 DOT Scalar Fluxes with TORT Scalar Fluxes Using the Original DOTTOR Algorithm	24
3.	Comparison of Group 1 DOT Scalar Fluxes with TORT Scalar Fluxes Using the Modified DOTTOR Algorithm	27
4.	Comparison of Group 2 DOT Scalar Fluxes with TORT Scalar Fluxes Using the Modified DOTTOR Algorithm	27
5.	Comparison of CPU Times for Original and Modified DOTTOR Algorithms	28
A.1.	Array Pointers, Corresponding Arrays, and Array Lengths for Common BIG	44
A.2.	Layout and Description of Variables in Common BIG	45
A.3.	Additional Subroutines Required by DOTTOR	46

ABSTRACT

A method has been developed to couple two-dimensional (2-D) to three-dimensional (3-D) discrete ordinates transport calculations. This method is useful for problems in which a 3-D Cartesian (X-Y-Z geometry) region of interest is very far from a point source. A 3-D solution from the source including the region of interest is prohibited due to the large computing cost of such calculations.

The problem is solved by first performing a 2-D discrete ordinates calculation from the source past the region of interest. The results of the 2-D calculations are transformed into a boundary condition on the surface of the 3-D region of interest. This transformation or coupling method is developed and implemented in the DOTTOR computer code. The boundary condition is then used for a subsequent 3-D discrete ordinates calculation in the region of interest.

Simple test problems were used to evaluate the accuracy and speed (i.e., computing cost) of the DOTTOR code. The evaluation indicates that the DOTTOR code produces accurate results with acceptable computing costs. The algorithm chosen showed a significant speed advantage over others tested when applied to large problems.

1. INTRODUCTION

A three-dimensional (3-D) discrete ordinates transport code,^{1,2} TORT, has been developed at the Oak Ridge National Laboratory for radiation (i.e., neutrons and photons) penetration studies. Thus far, TORT has been applied mainly to problems in which the dose is desired inside a concrete building. One problem of particular interest consists of determining the flux in a building located a large distance from a point source (see Fig. 1). It is not feasible to solve this particular problem with TORT because (1) the discretized 3-D problem is simply too large to fit on the computer or (2) the computing time (and corresponding cost) is prohibitive. For example, the building alone when modeled with 2×10^8 unknowns (i.e., a $100 \times 20 \times 30$ spatial mesh, 60 directions, and 60 energy groups) requires most of the available computer memory. Due to this computer memory limitation, it is impossible to include the radiation source, which may be located more than 100,000 cm from the building, in the 3-D building calculation. In addition, the building calculation alone requires several hours of central processing unit (CPU) time on a CRAY computer.

Fortunately, such problems can be solved with a hybrid approach by coupling a two-dimensional (2-D) description (cylindrical R-Z geometry) of the point source, which is assumed to be azimuthally symmetric, to a 3-D description (Cartesian geometry) of the building, the region of interest. This coupling methodology is described in the following steps:

1. perform a 2-D discrete ordinates calculation, using the DOT³ code, from the point source including the location of the 3-D region of interest,
2. normalize and reformat the 2-D directional fluxes from DOT using the VISTA code (see Appendix E),

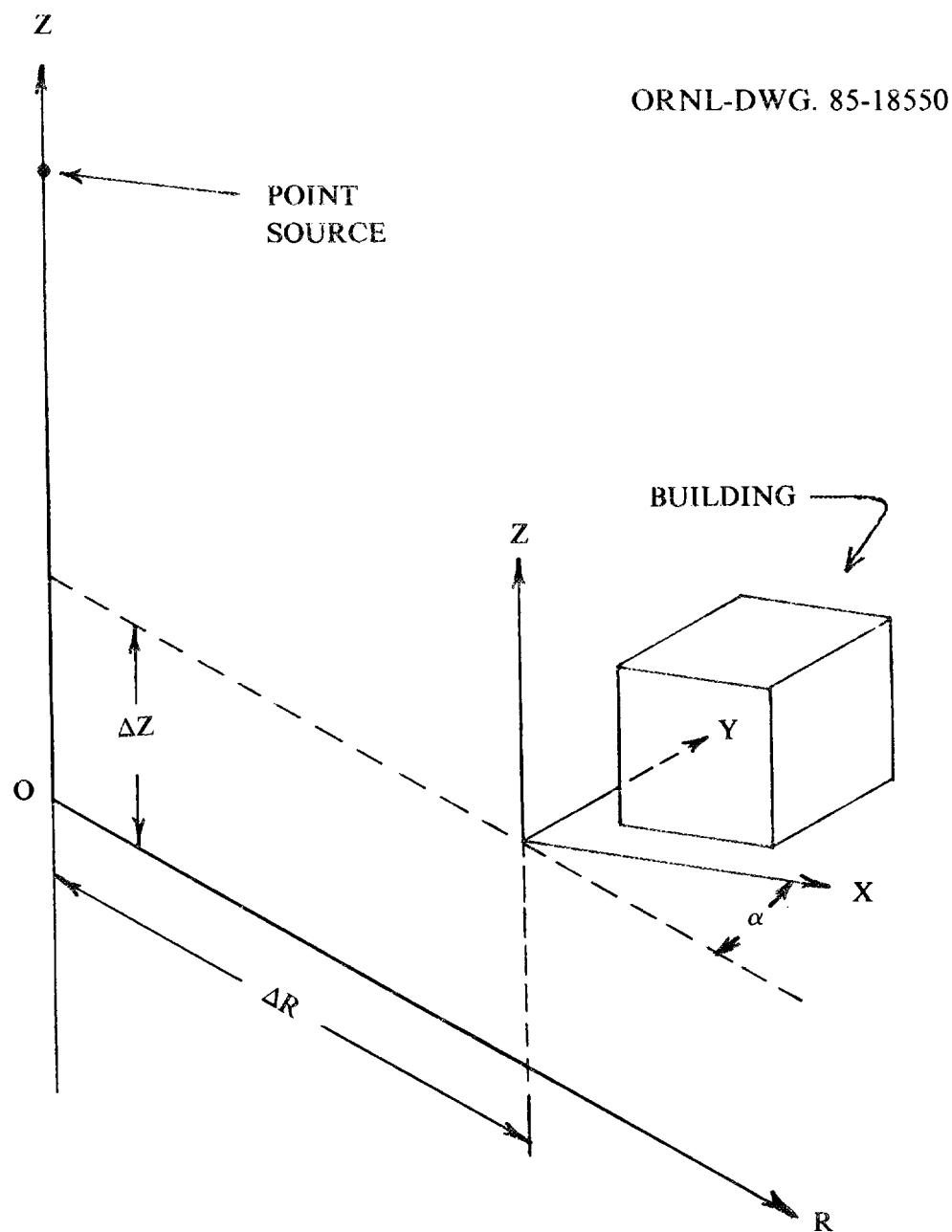


Fig. 1. Problem geometry

3. transform, or couple, the 2-D fluxes from the DOT/VISTA calculations into a fixed source boundary condition on the surface of the 3-D region using the DOTTOR (Discrete Orдинates to Three-dimensional Oak Ridge Transport) code,
4. perform a 3-D discrete ordinates calculation, using the TORT code, in the 3-D region using the boundary conditions from DOTTOR.

An advantage of this method is the ability to run several building calculations, each with different parameters, using only one source calculation. For example, steps 1 and 2 above can be run for a particular source configuration, then steps 3 and 4 can be repeated for different building locations, rotations (about the 3-D Z-axis), mesh sizes, etc.

Figure 2 shows the relationship between DOTTOR and the other codes used in this work. The 2-D to 3-D coupling methodology in step 3 above is the essence of this thesis and is described in Section 2. The implementation and evaluation of this methodology in the DOTTOR code is described in Section 3. Finally, a brief summary and the important conclusions of this work are presented in Section 4.

ORNL-DWG. 85-18551

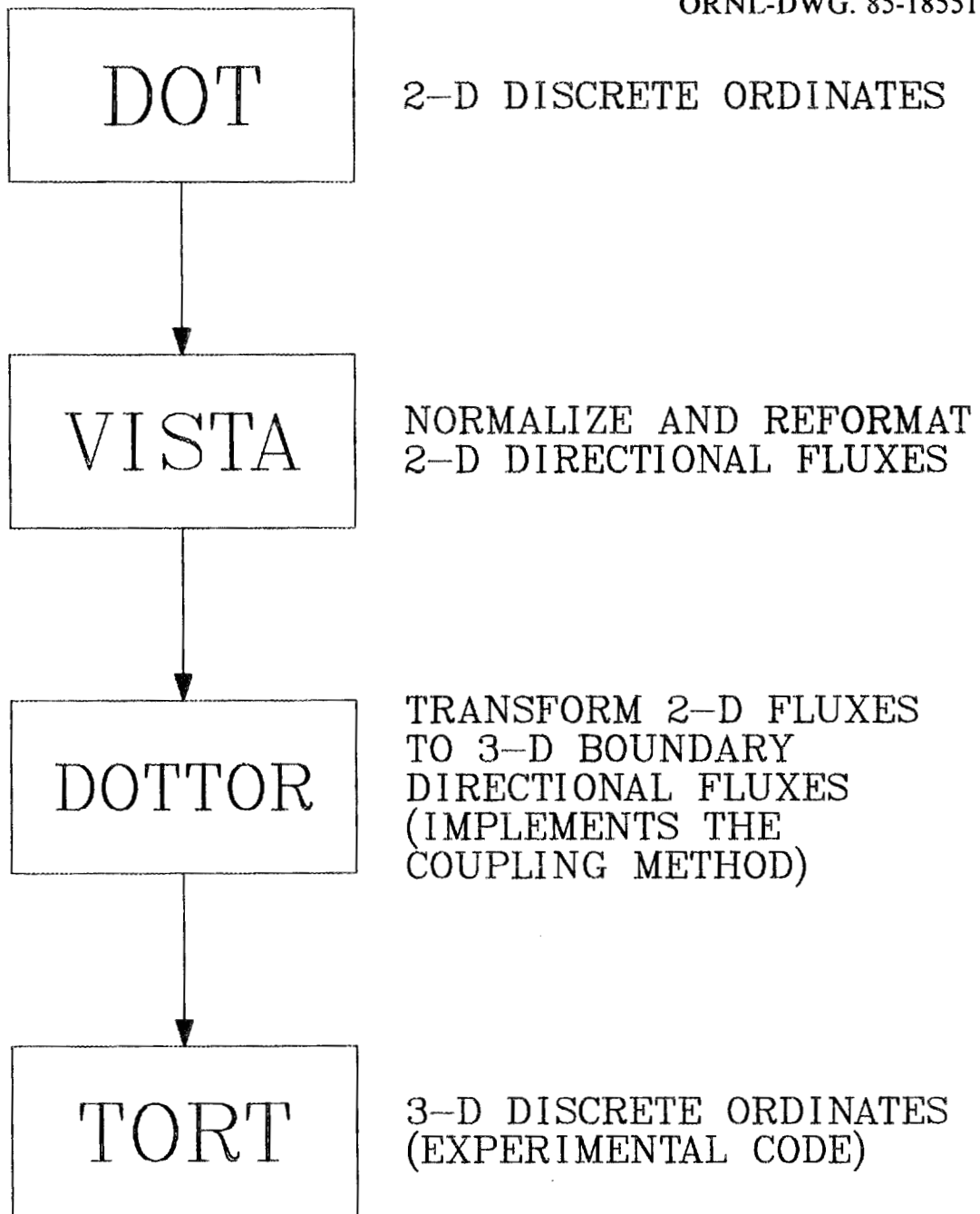


Fig. 2. Computer code relationships and functions

2. METHOD DEVELOPMENT

The boundary condition needed for the 3-D calculation consists of the inward directed directional flux on all six sides of the 3-D region. Transformation of the 2-D directional fluxes into the boundary condition involves the following steps:

1. determine the position in the 2-D mesh of a given point on the surface of the 3-D region,
2. transform the 2-D quadrature representation of the directional flux to a 3-D quadrature with the same or fewer directions,
3. rotate the 3-D quadrature relative to the 2-D quadrature to account for rotation of the 3-D coordinate system relative to the 2-D coordinate system,
4. perform a 2-D spatial interpolation between the four neighboring 2-D flux positions to determine a directional flux value for a given direction at a given point on the surface of the 3-D region.

The quadrature transformation in step 2 is necessary to reduce the cost and computer memory required in the 3-D TORT calculation.

2.1 POSITION DETERMINATION

The position in the 2-D mesh of a given point on the surface of the 3-D region must be found in order to determine the four neighboring 2-D mesh points. The position can be found using the geometry of the problem and the position of the 3-D mesh relative to the 2-D mesh. The following parameters are used to describe the position of the 3-D mesh in the 2-D mesh (see Fig. 1):

α = the angle measured counterclockwise from the 2-D radial axis to the 3-D X-axis,

ΔR = the radial distance from the 2-D origin to the 3-D origin,

ΔZ = the axial distance from the 2-D origin to the 3-D origin.

The 2-D R-axis direction may be different for each 3-D mesh point. In general, the angle α between the R-axis and X-axis is different for each 3-D mesh point (see Fig. 3). If the distance from the 2-D origin to the 3-D origin, ΔR , is large enough, α may be considered a constant for all 3-D mesh points. A large ΔR was assumed in order to simplify the initial computer code implementation.

For a given 3-D mesh point, the axial position, Z_T , in the 2-D mesh can be calculated from

$$Z_T = Z + \Delta Z , \quad (1)$$

where Z is the position along the 3-D Z-axis of the given point.

The radial position, R_T , in the 2-D mesh for a given 3-D point is found by first finding the position of the 2-D Z-axis, (X_D, Y_D) , in the 3-D X-Y plane. The following relationships are used (see Fig. 4):

$$X_D = \begin{cases} -\Delta R \cos\alpha, & 0 \leq \alpha \leq \frac{\pi}{2} \\ \Delta R \cos(\pi - \alpha), & \frac{\pi}{2} < \alpha \leq \pi \\ \Delta R \cos(\alpha - \pi), & \pi < \alpha \leq \frac{3\pi}{2} \\ -\Delta R \cos(2\pi - \alpha), & \frac{3\pi}{2} < \alpha \leq 2\pi \end{cases} \quad (2)$$

ORNL-DWG. 85-18552

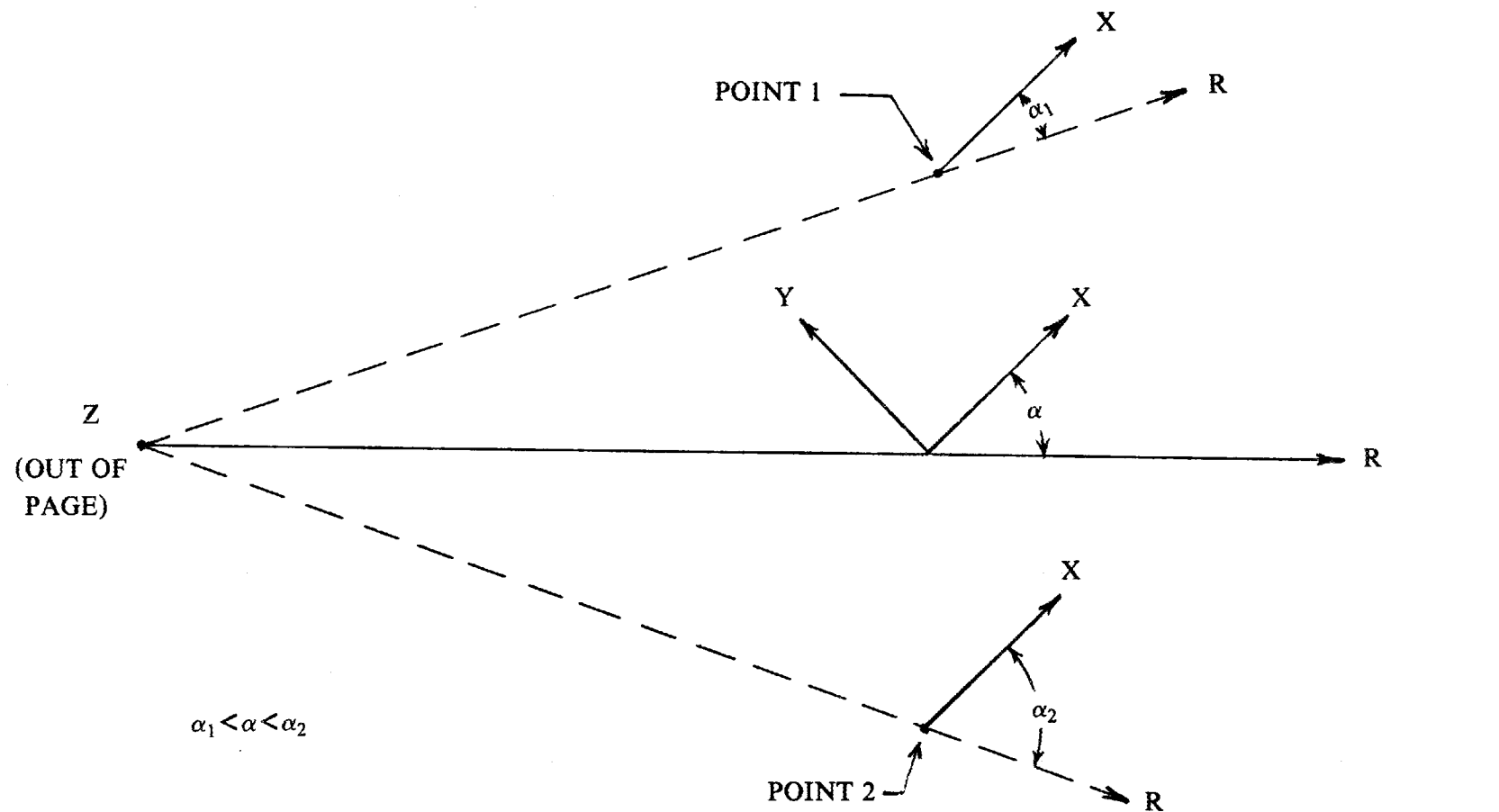
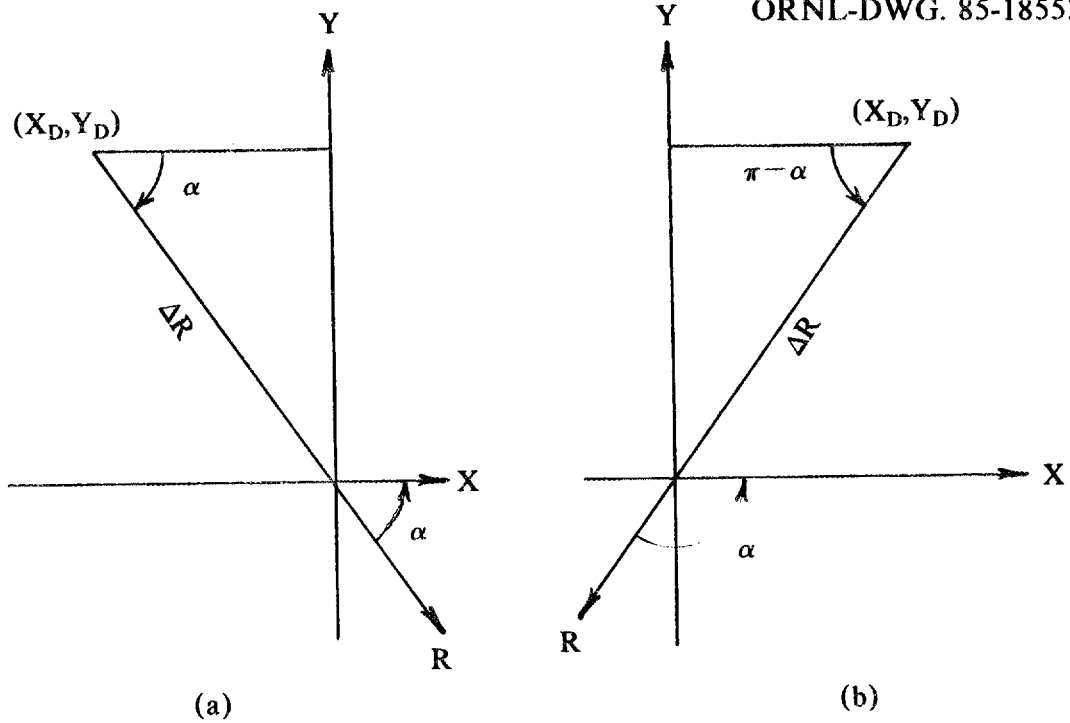
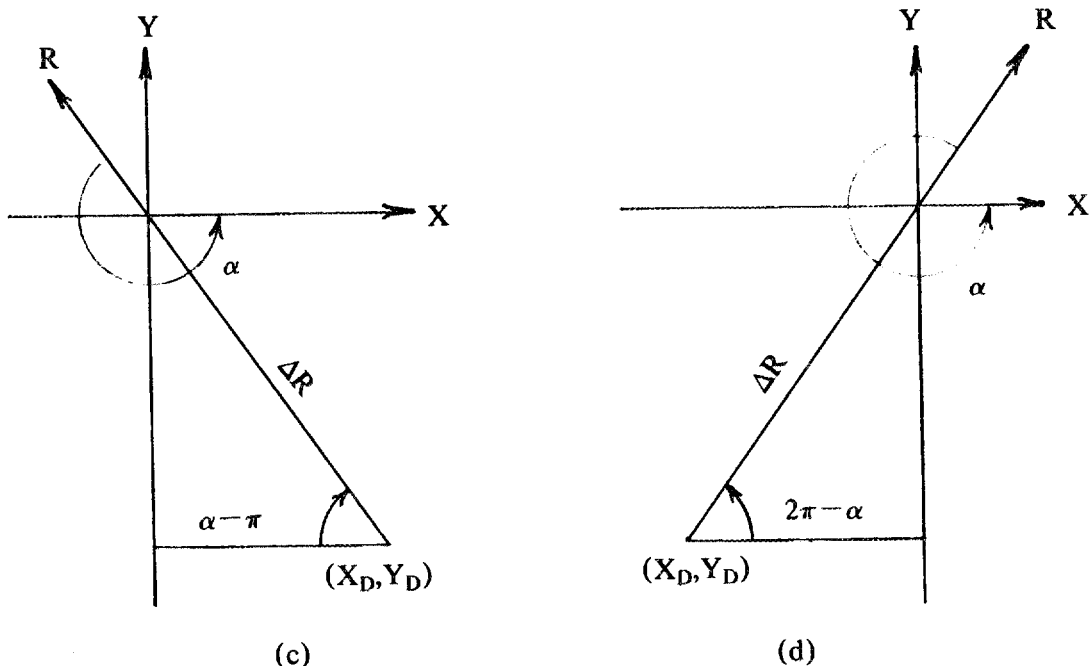


Fig. 3. Angle α varies for points on different radial vectors



(a)

(b)



(c)

(d)

Fig. 4. Position of the 2-D Z-axis (X_D, Y_D) , in the 3-D X-Y plane for

(a) $0 \leq \alpha \leq \frac{\pi}{2}$, (b) $\frac{\pi}{2} < \alpha \leq \pi$, (c) $\pi < \alpha \leq \frac{3\pi}{2}$, and (d) $\frac{3\pi}{2} < \alpha \leq 2\pi$

$$Y_D = \begin{cases} \Delta R \sin \alpha, & 0 \leq \alpha \leq \frac{\pi}{2} \\ \Delta R \sin(\pi - \alpha), & \frac{\pi}{2} < \alpha \leq \pi \\ -\Delta R \sin(\alpha - \pi), & \pi < \alpha \leq \frac{3\pi}{2} \\ -\Delta R \sin(2\pi - \alpha), & \frac{3\pi}{2} < \alpha \leq 2\pi \end{cases} \quad (3)$$

The distance formula is used to find R_T ,

$$R_T = [(X_D - X)^2 + (Y_D - Y)^2]^{1/2}, \quad (4)$$

where (X, Y) are the coordinates of the 3-D point in the 3-D X-Y plane.

Once found, the positions within the 2-D mesh, Z_T and R_T , are compared with the axial and radial 2-D mesh midpoints to find the four neighboring mesh positions which the given 3-D point lies between.

2.2 2-D TO 3-D QUADRATURE TRANSFORMATION

Quadrature is used to discretize the angular dependence of the flux.⁴ The quadrature set may be thought of as points on a unit sphere about a given spatial point. Each point on the sphere represents a discrete direction. Each discrete direction is described by the direction cosines of the unit vector from the given spatial point to the point on the surface of the unit sphere. Each direction has a weight associated with it which represents a fraction of the total solid angle of the sphere.

The direction $\bar{\Omega}_m$ is defined by

$$\bar{\Omega}_m = \mu_m \bar{i} + \xi_m \bar{j} + \eta_m \bar{k} \quad (5)$$

where μ_m = cosine of angle between $\bar{\Omega}_m$ and spatial direction \bar{i} ,

ξ_m = cosine of angle between $\bar{\Omega}_m$ and spatial direction \bar{j} ,

η_m = cosine of angle between $\bar{\Omega}_m$ and spatial direction \bar{k} .

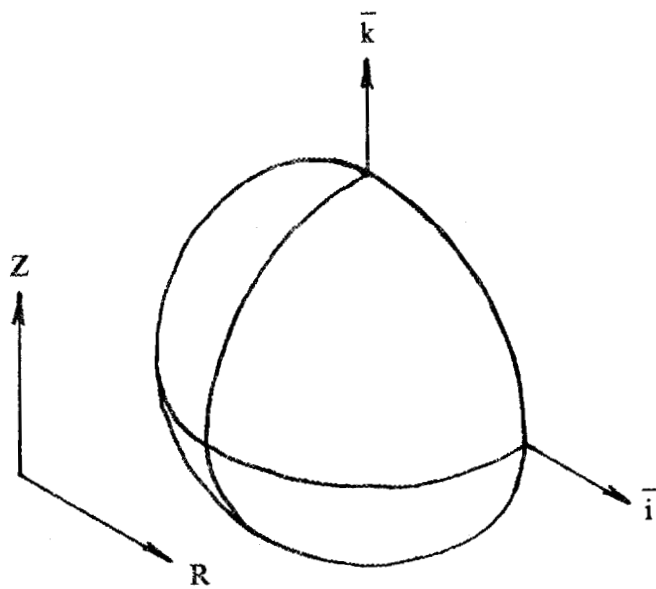
The quadrature set is defined by μ_m , ξ_m , η_m , and w_m for $m = 1, 2, 3, \dots, MM$, where w_m is the weight which represents a fraction of the total solid angle of the sphere and MM is the number of directions in the quadrature. Therefore, the weights w_m must satisfy

$$\sum_{m=1}^{MM} w_m = 1 . \quad (6)$$

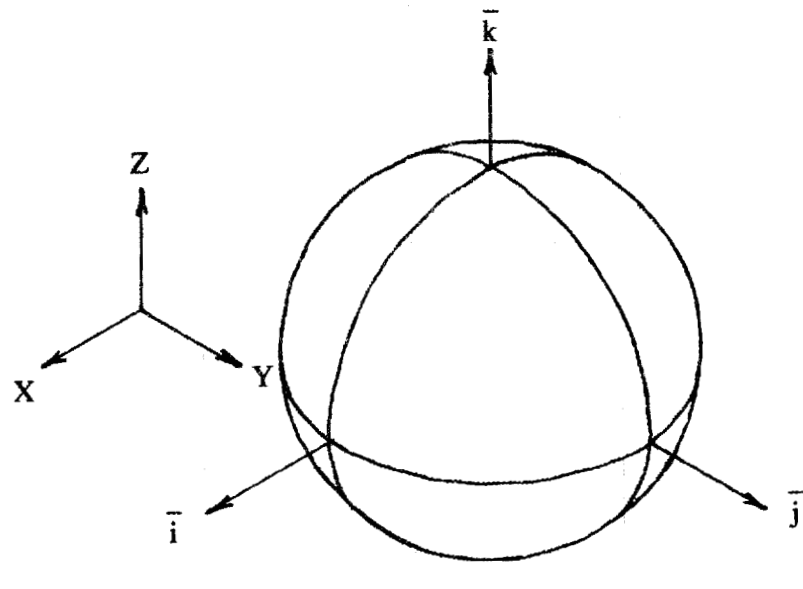
A one-dimensional quadrature requires only one of the direction cosines, a 2-D quadrature requires two direction cosines, and a 3-D quadrature requires all three direction cosines. A 2-D quadrature set can be thought of as points on a hemisphere with its center at the spatial point (see Fig. 5a). All points on the hemisphere can be represented by the direction cosines μ and η . A 3-D quadrature set can also be thought of as points on a sphere (see Fig. 5b). The weights for directions in a 2-D quadrature are normalized to the total solid angle of a hemisphere, 2π . The weights for directions in a 3-D quadrature are normalized to the total solid angle of a sphere, 4π .

Directional fluxes represented by a 2-D quadrature are directed toward only one side of the 2-D spatial plane, i.e., inside a hemisphere. In order to convert this representation to a 3-D quadrature representation, the "empty" hemisphere must be filled with directions. The "empty" hemisphere is assumed to be a mirror image of the 2-D hemisphere. The original 2-D fluxes are directed in only $-\xi$ directions. The directions in the new hemisphere will have the same μ and η values but will now have both $+\xi$ and $-\xi$ directions. The number of 3-D directions will be twice the number of 2-D directions.

ORNL-DWG. 85-18554



(a)



(b)

Fig. 5. Representation of (a) a 2-D quadrature, and (b) a 3-D quadrature

The weights for the new 3-D fluxes must be renormalized to 4π instead of 2π ; thus

$$w_m^{3D} = \frac{w_m^{2D}}{2} . \quad (7)$$

The 3-D flux values in the $-\xi$ directions are the same as the 2-D flux values. The 3-D flux values in the $+\xi$ directions are the same as the corresponding 2-D fluxes in the $-\xi$ directions or

$$\psi_m^{3D}(\mu_m, +\xi_m, \eta_m) = \psi_m^{2D}(\mu_m, -\xi_m, \eta_m) . \quad (8)$$

The 2-D directional fluxes have now been transformed into angular fluxes with a 3-D quadrature representation.

2.3 QUADRATURE ROTATION AND REDUCTION

The 3-D quadrature representation must be rotated about the \bar{k} direction because of the rotation of the 3-D coordinate system with respect to the 2-D coordinate system by the angle α . In addition, the 3-D quadrature representation of the 2-D spatial fluxes must be reduced to a 3-D quadrature with fewer directions than the original 2-D quadrature in order to reduce the computing cost of the 3-D calculation. The 3-D representation of the original 2-D quadrature, which was used in the DOT calculation, is referred to as the "large 3-D quadrature." The 3-D quadrature used in the TORT calculation is referred to as the "small 3-D quadrature."

These rotation and reduction tasks can be accomplished by describing the solid angle boundaries $(\phi_1, \phi_2, \theta_1, \theta_2)$ for the large 3-D quadrature and the small 3-D quadrature. The solid angle boundaries are calculated from the following solid angle relationship (see Fig. 6),

ORNL-DWG. 85-18555

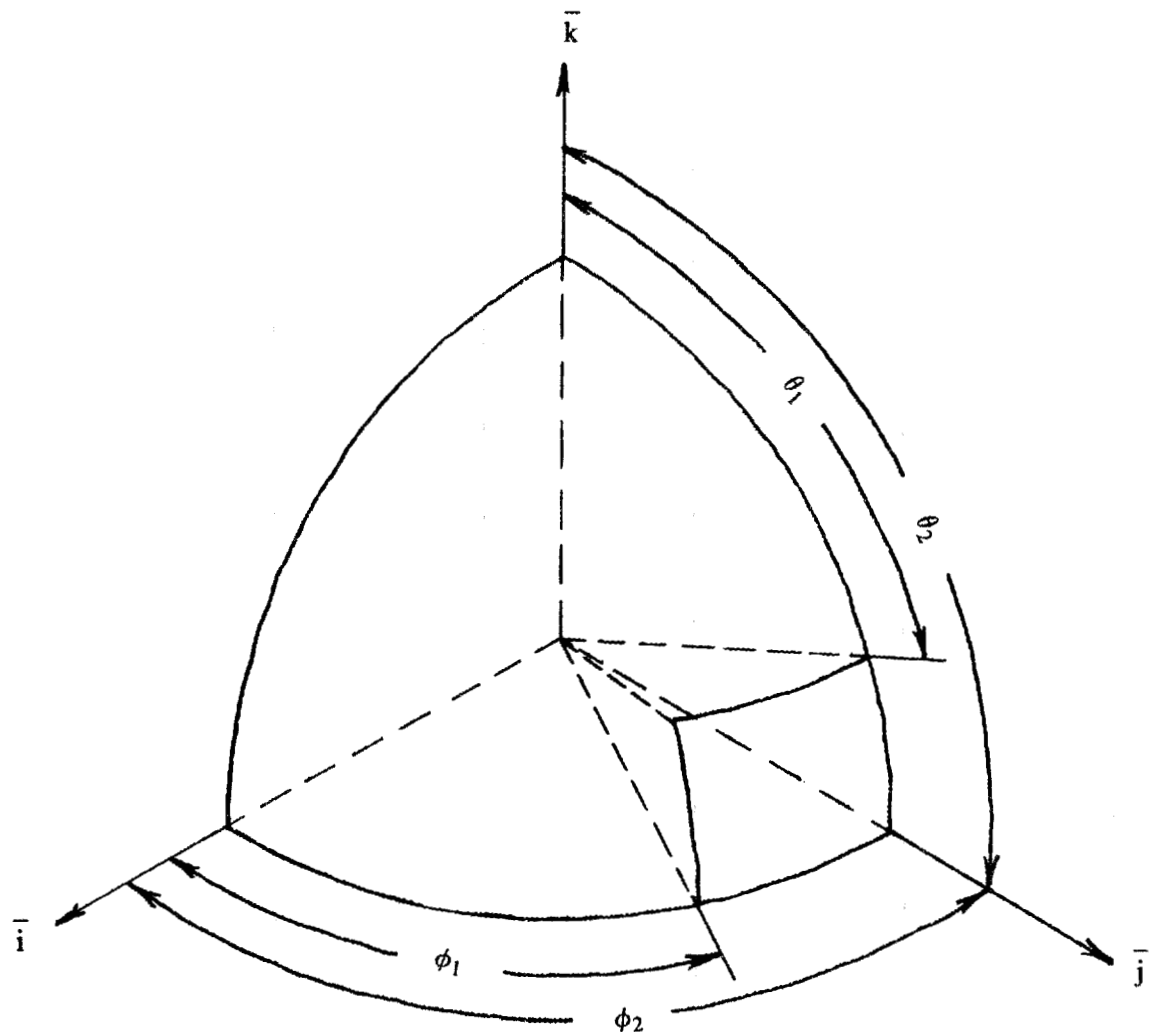


Fig. 6. Solid angle boundaries

$$SA = (\phi_2 - \phi_1)(\cos\theta_2 - \cos\theta_1) , \quad (9)$$

where

SA = solid angle in steradians,

ϕ_1 = azimuthal angle between \hat{i} and left boundary of the solid angle,

ϕ_2 = azimuthal angle between \hat{i} and right boundary of the solid angle,

θ_1 = polar angle between \hat{k} and upper boundary of the solid angle,

θ_2 = polar angle between \hat{k} and lower boundary of the solid angle.

This relationship can be rewritten as

$$SA = (\phi_2 - \phi_1)(\eta_2 - \eta_1) , \quad (10)$$

where $\eta_1 = \cos\theta_1$, and $\eta_2 = \cos\theta_2$.

If the following definitions are made,

$$\Delta\phi = \phi_2 - \phi_1 \text{ (azimuthal angle increment)}, \quad (11)$$

$$\text{and } \Delta\eta = \eta_2 - \eta_1 \text{ (eta increment)}, \quad (12)$$

then the solid angle relationship can be written as

$$SA = \Delta\phi\Delta\eta . \quad (13)$$

The weight for a direction in a 3-D quadrature is given by

$$w_m^{3D} = \frac{SA_m}{4\pi} = \frac{\Delta\phi_m \Delta\eta_m}{4\pi} . \quad (14)$$

The values of $\Delta\phi$ and $\Delta\eta$ for each direction are unknown and must be calculated. This is a simple calculation if the quadratures are level symmetric which means that the values of $\Delta\eta$ are the same for all directions with the same η value. All directions with the same η value make up an eta level (see Fig. 7).

By limiting the directions considered to only one octant, the $\Delta\eta$ for an eta level l is calculated as follows:

$$\sum_m w_m^{3D} = \sum_m \frac{\Delta\phi_m \Delta\eta_l}{4\pi} ; m \text{ in level } l \quad (15)$$

$$= \frac{\Delta\eta_l}{4\pi} \sum_m \Delta\phi_m .$$

Since one octant is considered,

$$\sum_m \Delta\phi_m = \frac{\pi}{2} , \quad (16)$$

then

$$\sum_m w_m^{3D} = \frac{\Delta\eta_l \cdot \pi}{4\pi \cdot 2} \quad (17)$$

$$= \frac{\Delta\eta_l}{8} ,$$

or

$$\Delta\eta_l = 8 \sum_m w_m^{3D} . \quad (18)$$

Once the $\Delta\eta$ value for each direction within an eta level is known, the $\Delta\phi$ value for each direction is calculated from

ORNL-DWG. 85-18556

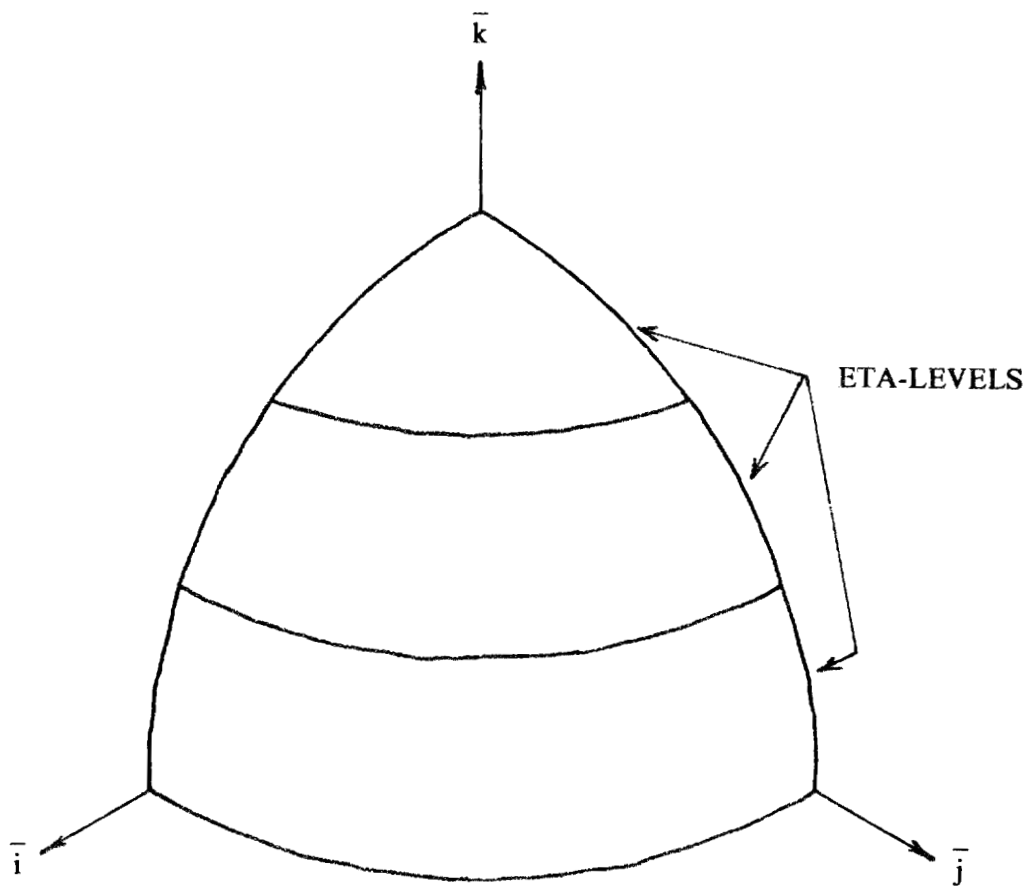


Fig. 7. Eta levels in a level symmetric quadrature

$$\Delta\phi_m = \frac{4\pi w_m^{3D}}{\Delta\eta_m} . \quad (19)$$

This method of calculating $\Delta\phi$ and $\Delta\eta$ is based on a technique used in the subroutine BINR,⁵ but modified here for use with 3-D quadratures.

The rotation angle α and the solid angle boundaries are used to rotate and reduce the 2-D quadrature flux representation. The small 3-D quadrature is rotated about the \bar{k} direction an amount α relative to the 2-D quadrature. The solid angle boundaries for a given small 3-D quadrature are compared to the solid angle boundaries for the large 3-D quadrature. The fluxes for the large quadrature directions overlapped by the given small quadrature direction are used to calculate the 3-D directional flux for the given small quadrature direction. The directional flux in the given small quadrature direction is conserved. The following equation is used to calculate the flux for the given small quadrature direction (see Fig. 8).

$$\psi_m^{S3D} = \frac{1}{w_m^{S3D}} \sum_l \sum_n f_{lnm} \psi_{ln}^{L3D} w_{ln}^{L3D} , \quad (20)$$

where ψ_m^{S3D} = desired flux for direction m in the small 3-D quadrature,

w_m^{S3D} = weight for direction m in the small 3-D quadrature,

ψ_{ln}^{L3D} = flux for direction n of eta level l in the large 3-D quadrature,

f_{lnm} = fraction of solid angle for large 3-D quadrature direction n of eta level l overlapped by the small 3-D quadrature direction m,

w_{ln}^{L3D} = weight for direction n of eta level l in the large quadrature.

ORNL-DWG. 85-18557

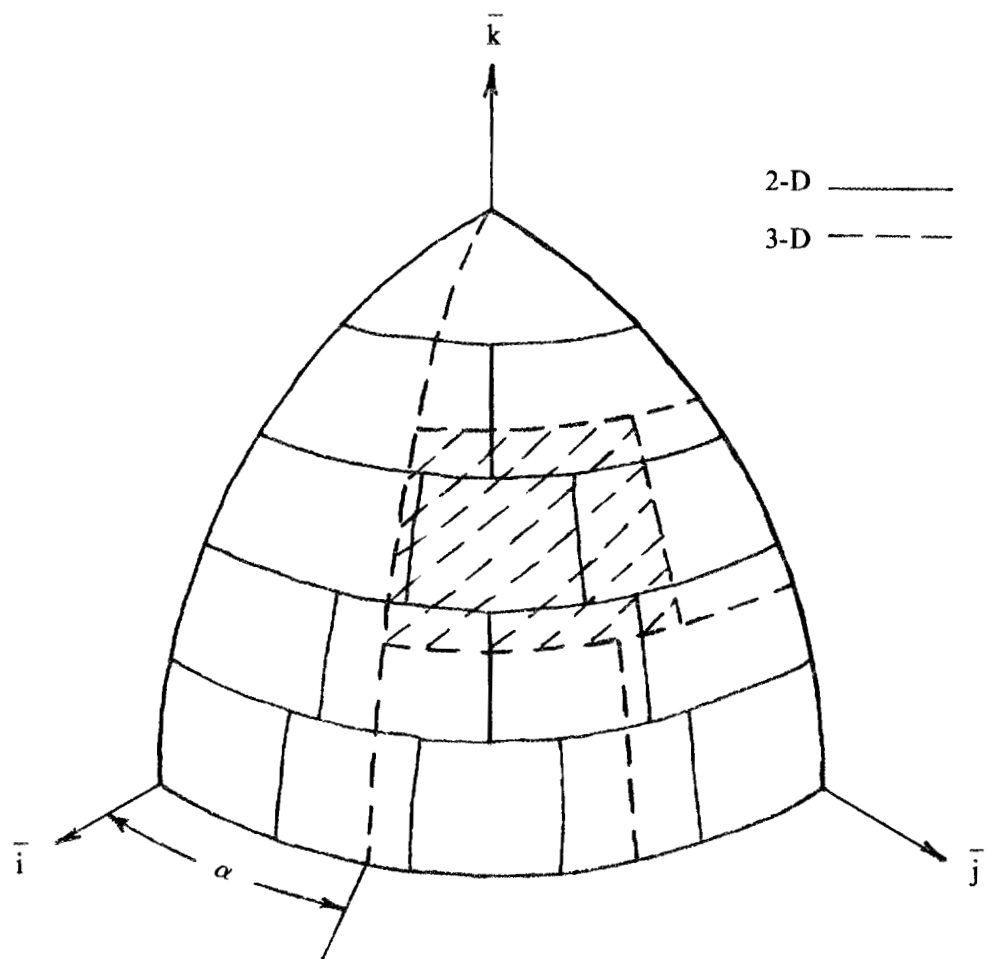


Fig. 8. Quadrature reduction and rotation

The f_{lmn} values are calculated from

$$f_{lmn} = \frac{\text{SA of direction } n \text{ of eta level } l \text{ overlapped by direction } m}{\text{total SA of direction } n} . \quad (21)$$

For a given small quadrature direction, four of these reduced and rotated flux values are calculated. These four flux values correspond to the four neighboring 2-D mesh positions.

2.4 SPATIAL INTERPOLATION

The directional flux value at the desired 3-D point is calculated by performing a 2-D linear interpolation between the four neighboring flux points previously calculated (see Fig. 9). The equation for this interpolation can be obtained by first defining two intermediate flux points ψ_{T1} and ψ_{T2} . The flux values for these points are obtained by linear interpolation in the radial direction.

$$\psi_{T1} = \frac{(R_T - R_1)}{(R_2 - R_1)} \psi_2 + \frac{(R_2 - R_T)}{(R_2 - R_1)} \psi_1 , \quad (22)$$

$$\psi_{T2} = \frac{(R_T - R_1)}{(R_2 - R_1)} \psi_4 + \frac{(R_2 - R_T)}{(R_2 - R_1)} \psi_3 . \quad (23)$$

The value of the flux at the desired point, ψ_T , is given by

$$\psi_T = \frac{(Z_2 - Z_T)}{(Z_2 - Z_1)} \psi_{T1} + \frac{(Z_T - Z_1)}{(Z_2 - Z_1)} \psi_{T2} . \quad (24)$$

ORNL-DWG. 85-18558

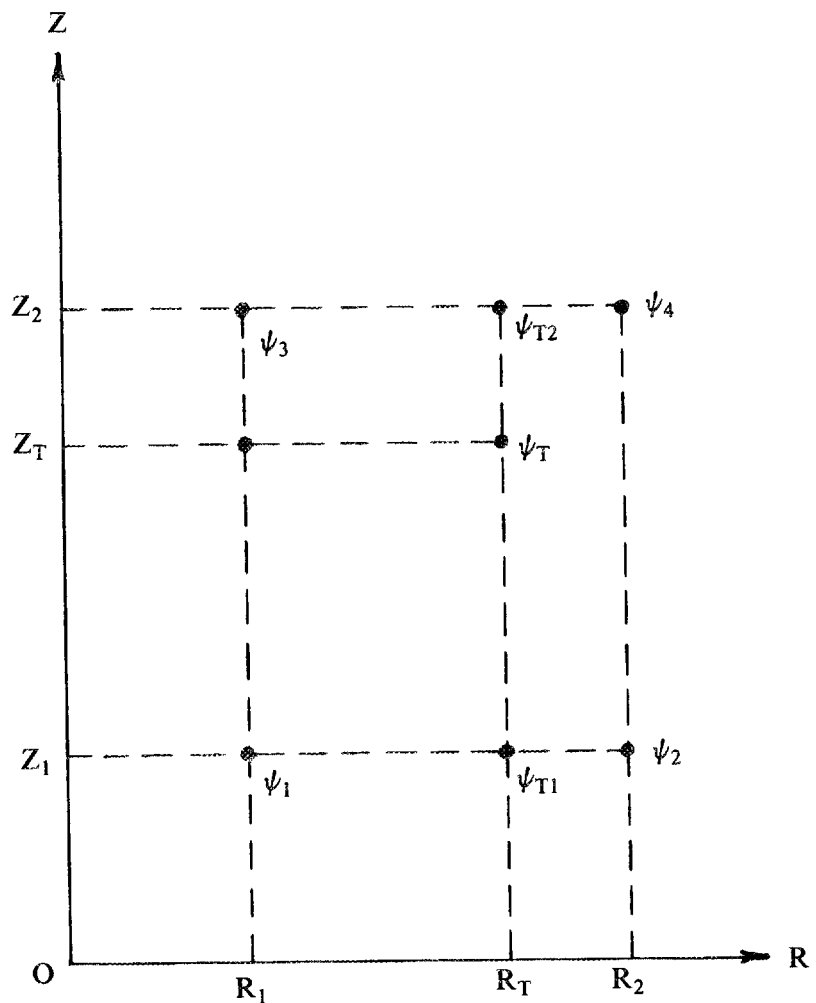


Fig. 9. Spatial interpolation

Substituting the expressions for ψ_{T1} and ψ_{T2} , the result is

$$\begin{aligned}\psi_T &= \frac{(R_2 - R_T)(Z_2 - Z_T)}{(R_2 - R_1)(Z_2 - Z_1)}\psi_1 + \frac{(R_T - R_1)(Z_2 - Z_T)}{(R_2 - R_1)(Z_2 - Z_1)}\psi_2 \\ &\quad + \frac{(R_2 - R_T)(Z_T - Z_1)}{(R_2 - R_1)(Z_2 - Z_1)}\psi_3 + \frac{(R_T - R_1)(Z_T - Z_1)}{(R_2 - R_1)(Z_2 - Z_1)}\psi_4.\end{aligned}\quad (25)$$

3. METHOD IMPLEMENTATION AND EVALUATION

The 2-D to 3-D coupling method is implemented in the DOTTOR computer code. A detailed description of DOTTOR is given in Appendix A, input data is described in Appendix B, and a sample problem with input and output is given in Appendix C.

The DOTTOR code was evaluated for both accuracy and speed of operation. Accuracy was evaluated by first performing a 2-D DOT calculation in R-Z geometry. The directional fluxes from the DOT calculation are then normalized and reformatted by the VISTA code. The DOTTOR code transforms the 2-D directional fluxes from VISTA into a boundary condition on the surface of a 3-D region. The fluxes inside the 3-D region are calculated by the TORT code using the 3-D boundary condition determined by DOTTOR. The material in the 3-D TORT region and also in the 2-D DOT calculation is the same--namely, air. Thus, if the boundary condition calculated by DOTTOR is correct, the 3-D TORT and 2-D DOT fluxes should be in good agreement.

The DOT calculation is an air-over-ground problem consisting of a 48 x 57 2-D R-Z mesh, S8 quadrature (48 directions), and two energy groups with the air/ground interface at Z=0. The boundaries of the DOT problem extended from -243.84 cm to 100,000 cm axially and from 0.0 cm to 100,000 cm radially. The 3-D coordinate system origin is placed at a radial position (ΔR) of 610 cm and an axial position (ΔZ) of 100 cm. The counterclockwise angular rotation (α) of the 3-D X-axis relative to the 2-D R-axis is 45 degrees. The 3-D mesh is 10 x 9 x 9 with the X-boundaries extending from -220 cm to 220 cm, the Y-boundaries extending from -170 cm to 170 cm, and the Z-boundaries extending from -30 cm to 320 cm. The 2-D S8 quadrature (48 directions) was reduced to a 3-D S6 quadrature (60 directions).

After all calculations were completed, the scalar flux from the 3-D TORT calculation was compared to the scalar flux at the corresponding 2-D mesh point. Since

the 2-D and 3-D mesh points do not coincide, a spatially interpolated flux value was used for the 2-D value.

The results of the comparison show that the TORT scalar flux values are generally within 1.0% of the interpolated DOT scalar fluxes. (Some of the results are shown in Tables 1 and 2.) The close agreement of the TORT and DOT results indicate that the DOTTOR code is performing correctly.

DOTTOR uses only a few seconds of central processing unit (CPU) time for small problems about the size of the test problem used for evaluation. However, for large practical problems the CPU time can be much larger. For example, a problem with a $117 \times 33 \times 27$ 3-D mesh, 240 to 60 direction reduction, and 58 energy groups takes about 30 minutes of CPU time on a CRAY computer.

In order to reduce the cost for large problems, an effort was made to reduce the CPU time required. The overall DOTTOR algorithm was reviewed for possible modifications which would speed up its operation.

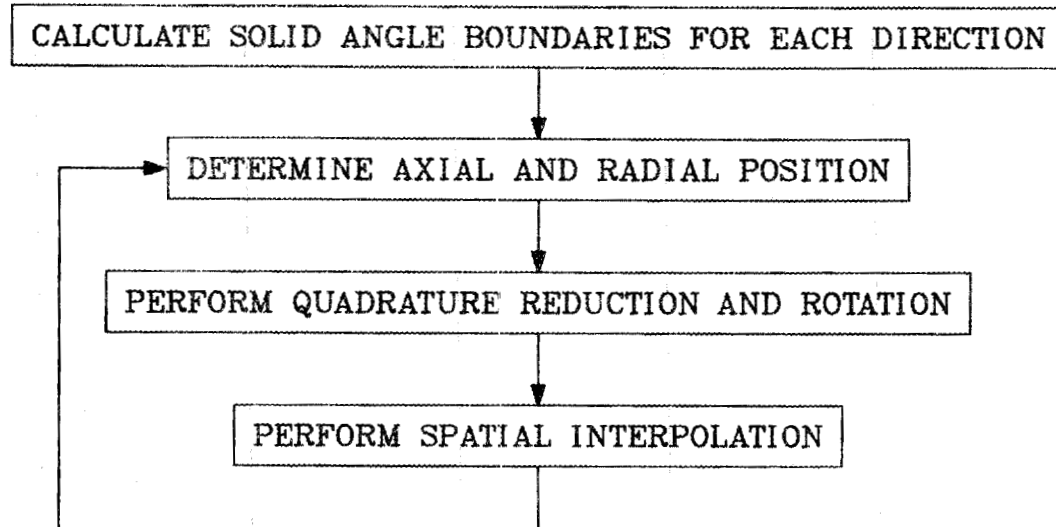
The DOTTOR algorithm performs the quadrature reduction and rotation at each spatial mesh point on the surface of the 3-D region. For a $100 \times 20 \times 30$ 3-D mesh size the number of spatial points is 5,600. Large practical problems usually require 2-D angular flux information from a spatial mesh no larger than 10×10 , or 100 spatial points. If the quadrature reduction and rotation operations are separated, the reduction operation alone can be applied to the 10×10 mesh of 2-D fluxes for a savings of 5,500 reduction operations. The rotation operations can then be performed at each of the 3-D mesh points separately. This allows the unique rotation angle, α , at each 3-D mesh point to be used in the rotation calculation. The requirement that ΔR be large is not necessary with the new algorithm. Figure 10 shows a comparison of the original and new algorithms.

Table 1. Comparison of Group 1 DOT Scalar Fluxes with TORT Scalar Fluxes Using the Original DOTTOR Algorithm

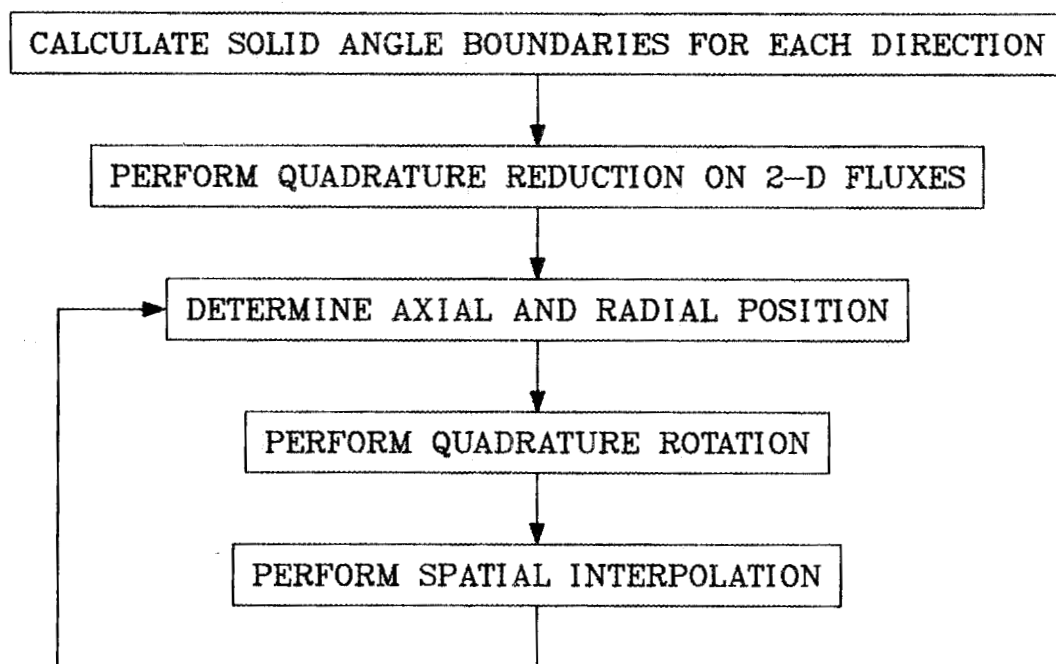
3-D mesh point (I, J, K)	DOT scalar flux	TORT scalar flux	$\Delta\%$
1 5 5	2.227E-11	2.227E-11	0.00
10 5 5	2.193E-11	2.199E-11	0.27
6 1 5	2.194E-11	2.200E-11	0.27
6 9 5	2.223E-11	2.221E-11	-0.09
6 5 1	2.164E-11	2.181E-11	0.79
6 5 9	2.254E-11	2.251E-11	-0.13
6 5 5	2.210E-11	2.216E-11	0.27

Table 2. Comparison of Group 2 DOT Scalar Fluxes with TORT Scalar Fluxes Using the Original DOTTOR Algorithm

3-D mesh point (I, J, K)	DOT scalar flux	TORT scalar flux	$\Delta\%$
1 5 5	7.928E-12	7.937E-12	0.11
10 5 5	7.863E-12	7.883E-12	0.25
6 1 5	7.866E-12	7.884E-12	0.23
6 9 5	7.921E-12	7.927E-12	0.08
6 5 1	7.694E-12	7.767E-12	0.95
6 5 9	8.076E-12	8.065E-12	-0.14
6 5 5	7.896E-12	7.923E-12	0.34



(a)



(b)

Fig. 10. Comparison of (a) original and (b) modified DOTTOR algorithms

This new algorithm was implemented in the DOTTOR code. The numerical results of the test problem for the new algorithm are shown in the Tables 3 and 4. Several problems were run with both the original and new algorithms. The CPU time required for the problems is compared in Table 5. For small problems the CPU time required for the new algorithm was greater than the old with the times approaching the same value as the mesh size of the problem increased.

One problem was run with a $10 \times 9 \times 9$ mesh, 240 to 60 direction reduction, and 58 energy groups. For this many-direction, many-group problem the CPU time for the new algorithm was less than half the time for the original algorithm. Use of the new algorithm is justified since it is faster for the larger, more costly problems to which the code is to be applied.

Table 3. Comparison of Group 1 DOT Scalar Fluxes with TORT Scalar Fluxes Using the Modified DOTTOR Algorithm

3-D mesh point (I, J, K)	DOT scalar flux	TORT scalar flux	$\Delta\%$
1 5 5	2.227E-11	2.216E-11	-0.49
10 5 5	2.193E-11	2.190E-11	-0.14
6 1 5	2.194E-11	2.190E-11	-0.18
6 9 5	2.223E-11	2.210E-11	-0.58
6 5 1	2.164E-11	2.158E-11	-0.28
6 5 9	2.254E-11	2.251E-11	-0.13
6 5 5	2.210E-11	2.202E-11	-0.36

Table 4. Comparison of Group 2 DOT Scalar Fluxes with TORT Scalar Fluxes Using the Modified DOTTOR Algorithm

3-D mesh point (I, J, K)	DOT scalar flux	TORT scalar flux	$\Delta\%$
1 5 5	7.928E-12	7.906E-12	-0.28
10 5 5	7.863E-12	7.855E-12	-0.10
6 1 5	7.866E-12	7.856E-12	-0.13
6 9 5	7.921E-12	7.894E-12	-0.34
6 5 1	7.694E-12	7.706E-12	0.16
6 5 9	8.076E-12	8.063E-12	-0.16
6 5 5	7.896E-12	7.880E-12	-0.20

Table 5. Comparison of CPU Times for Original and Modified DOTTOR Algorithms

Problem mesh size, directions, groups ^a	CPU time (sec.)		
	Original DOTTOR	Modified DOTTOR	time ratio (new/old)
5x3x3, 96-60, 2	0.88	1.28	1.45
10x9x9, 96-60, 2	3.03	3.48	1.15
19x19x19, 96-60, 2	10.55	11.32	1.07
10x9x9, 240-60, 58	96.23	44.66	0.46

^aMesh size refers to the 3-D mesh size, directions refer to the quadrature reduction performed by DOTTOR (e.g., 96-60 represents 96 directions used in the DOT calculation reduced to 60 directions for the TORT calculation), groups refers to the number of energy groups in the problem.

4. SUMMARY, CONCLUSIONS, AND FUTURE WORK

The 3-D TORT code cannot solve some radiation penetration problems such as determining the dose in a building located a large distance from a point source. However, this type of problem can be solved with a hybrid methodology in which a 2-D DOT calculation is coupled to a 3-D TORT calculation (see Sections 1 and 2). The methodology allows the 3-D quadrature used in the TORT calculation to have the same or fewer directions than the 2-D DOT quadrature. Also, the methodology accounts for angular rotations of the 3-D coordinate system relative to the 2-D coordinate system.

The coupling methodology has been implemented in the DOTTOR computer code (see Section 3 and Appendix A). Evaluation of DOTTOR using simple test problems produced excellent results. A comparison of the TORT scalar fluxes with the corresponding DOT scalar fluxes showed agreement within 1%. An effort was made to restructure the DOTTOR algorithm in order to decrease the CPU time required by DOTTOR. For large problems, the CPU time required by the modified algorithm was reduced to about half that of the original algorithm.

Future work on the DOTTOR code includes vectorization to further increase the speed on vector computers. Also, DOTTOR will be modified to allow the MORSE⁶ Monte Carlo code to use the boundary fluxes calculated by DOTTOR. Presently, the DOMINO^{7,8} code allows coupling of DOT R-Z geometry calculations to MORSE calculations. However, the DOMINO coupling is limited to cylindrical and disk surfaces centered about the DOT Z-axis. By using DOTTOR to perform the coupling, the MORSE calculation can be performed in a Cartesian region which is offset from the DOT Z-axis.

In conclusion, results of the DOTTOR evaluation demonstrate that the coupling methodology developed in Sections 1 and 2 works properly. More importantly, this methodology makes feasible the solution of some 3-D transport problems which would otherwise be impossible to obtain.

LIST OF REFERENCES

1. W. A. Rhoades, R. L. Childs, M. B. Emmett, and S. N. Cramer, "Applications of the Three-Dimensional Oak Ridge Transport Code," Proc. Am. Nucl. Soc. Topical Meeting on Reactor Physics and Shielding, September 17-19, 1984, Chicago.
2. R. L. Childs and W. A. Rhoades, "The Extension of the Linear Nodal Method to Large Concrete Building Calculations" (to be published).
3. W. A. Rhoades and R. L. Childs, "An Updated Version of the DOT 4 One- and Two-Dimensional Neutron/Photon Transport Code," ORNL-5851 (1982).
4. J. P. Jenal et. al., "The Generation of a Computer Library for Discrete Ordinates Quadrature Sets," ORNL/TM-6023 (1977).
5. M. B. Emmett and W. A. Rhoades, "CARP, A Computer Code and Albedo Data Library for Use by BREESE, the MORSE Albedo Package," ORNL/TM-6503 (1978).
6. M. B. Emmett, "The MORSE Monte Carlo Radiation Transport Code System," ORNL-4972 (1975).
7. M. B. Emmett, C. E. Burgart, and T. J. Hoffman, "DOMINO, A General Purpose Code for Coupling Discrete Ordinates and Monte Carlo Radiation Transport Calculations," ORNL-4853 (1973).
8. M. B. Emmett, "DOMINO-II, A General Purpose Code for Coupling DOT-IV Discrete Ordinates and Monte Carlo Radiation Transport Calculations," ORNL/TM-7771 (1981).
9. B. M. Carmichael, "Standard Interface Files and Procedures for Reactor Physics Codes, Version III," LA-5486-MS (1974).

APPENDICES

APPENDIX A

CODE DESCRIPTION

The DOTTOR code couples 2-D DOT fluxes in R-Z geometry to the surface of a 3-D X-Y-Z geometry region of interest. This coupling method is useful for shielding problems where

1. the source is a point (2-D R-Z geometry),
2. a 3-D discrete ordinates solution is desired in a 3-D region of interest (X-Y-Z geometry),
3. the source is some distance from the 3-D region of interest.

A 3-D solution from the source through the region of interest is prohibited by computing cost and geometry considerations.

The problem is solved by first obtaining a 2-D R-Z discrete ordinates solution from the source past the region of interest using the discrete ordinates code DOT. The flux output files from DOT are reformatted by the VISTA code and rewritten to a new file. The DOTTOR code uses the VISTA file to calculate the 3-D boundary directional fluxes on the region of interest. These boundary fluxes are written to another file. The 3-D discrete ordinates code TORT uses the DOTTOR boundary fluxes as a boundary condition for the 3-D calculation in the region of interest. Figure A.1 shows the relationship between the codes and their input/output files.

The DOTTOR code consists of three major routines and several additional routines for memory allocation and input/output (I/O) functions. The three major routines are the MAIN program, subroutine GETDAT, and subroutine INTERP. These routines are written in FORTRAN.

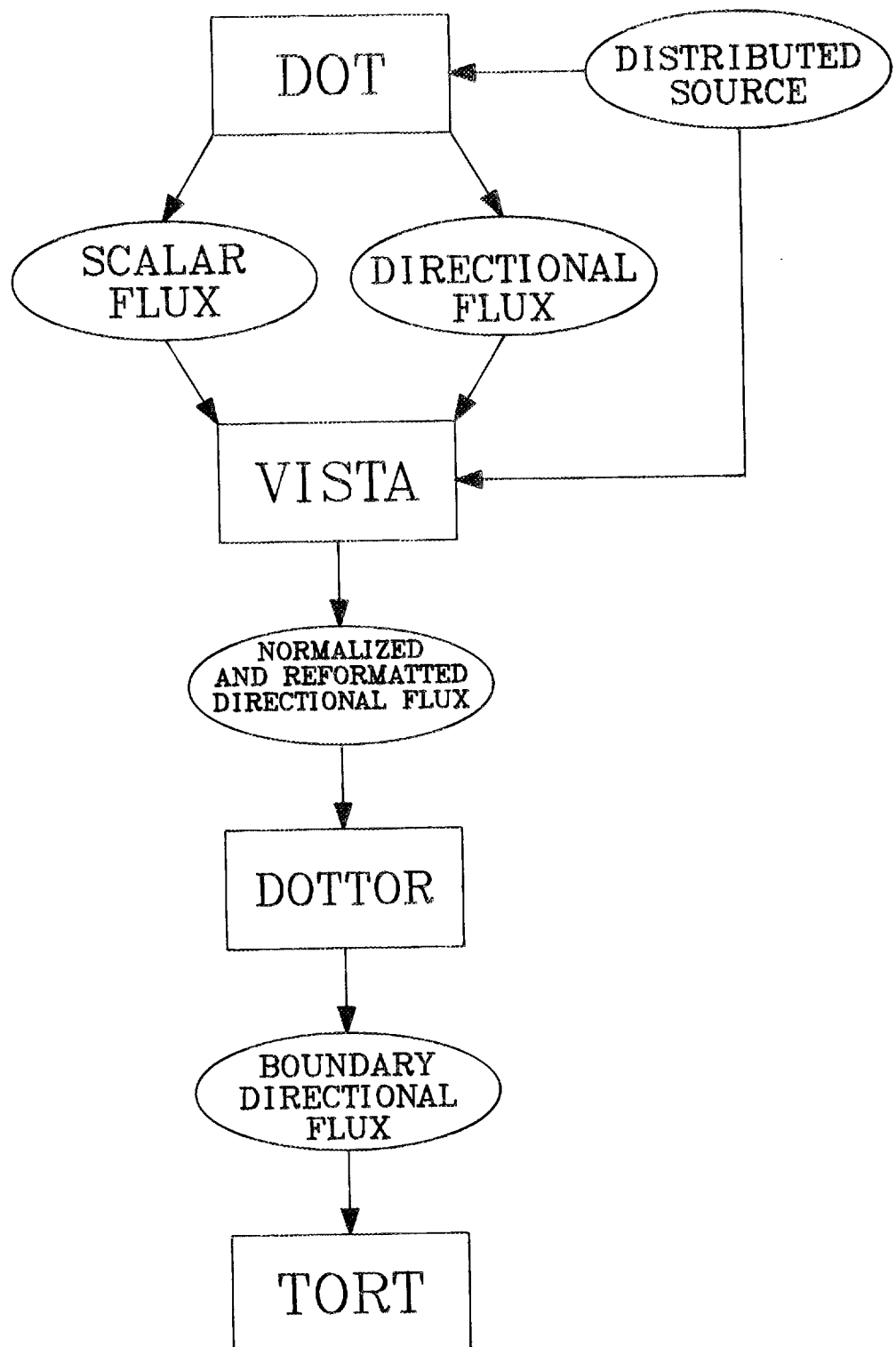


Fig. A.1. Computer codes used and their I/O files

The main program performs some initialization functions, reads the integer input data, and calls subroutine GETDAT. Subroutine GETDAT performs more initialization, reads both integer and real arrays from the VISTA output file, and reads the real input data. Subroutine INTERP is called from GETDAT. INTERP reads the 2-D fluxes from the VISTA file, performs the coupling to the 3-D surface, and writes the results to a file. A detailed description of the routines is given under Subroutine Descriptions.

The three routines share one common block entitled BIG. Common BIG contains integer array pointers and integer input data. Common BIG and its layout are described in more detail later. Also, a list and short description of the additional routines required to run the code are given later.

MAIN PROGRAM

The main program in DOTTOR does some preliminary initialization required for reading data from the VISTA output file. Standard input and output units are set to five and six, respectively. The default unit numbers for the VISTA output and DOTTOR output files are set to 20 and 21, respectively. The descriptive title, integer input (1\$\$ array), and TORT mesh position (2** array) are read and echoed to the standard output unit. The integer input (1\$\$ array) and TORT mesh position (2** array) are read using the FIDOS input routine. Subroutine GETDAT is called through subroutine DLOCAF.

Commons: BIG

Routines called: HEADER, COMFIX, CLEARX, DLOCAL, FIDOS, DLOCAF

SUBROUTINE GETDAT

Subroutine GETDAT reads the integer data from the VISTA output file into common BIG and echoes these values to the output unit. The VISTA integer data, the integer values in the 1\$\$ array, and additional constants are used to define the container array pointers in common BIG. The DOT quadrature and spatial mesh are read by calls to subroutine SEQIO. The TORT spatial mesh (3** input array) and three-dimensional quadrature (16**, 17**, and 18** input arrays) are read by a call to the FIDOS routine. The length of the container array LA is stored in variable LAEND. This length is compared to the available storage, LIMD, and the program execution is terminated if adequate storage is not available. Finally, the interpolation routine INTERP is called.

Commons: **BIG**

Called from: **DLOCAF**

Routines called: **DOPC, SEQIO, FIDOS, INTERP, WOT10, ALOCAF**

Argument list: (**LA, LIMD**)

SUBROUTINE INTERP

Subroutine INTERP reads the 2-D fluxes from the VISTA file and calculates 3-D TORT boundary fluxes. The 2-D quadrature is reduced during the transformation to a 3-D quadrature with fewer or equal directions. The 3-D boundary fluxes with reduced quadrature representation are then written to a file in TORT boundary directional file format.⁹

Subroutine INTERP first constructs a new 3-D quadrature equivalent to the 2-D quadrature used in the DOT calculation. This new quadrature has twice the number of

directions as the 2-D quadrature. The new 3-D quadrature is referred to as the "large" quadrature since the number of directions in it is greater than or equal to the number of directions in the "small" quadrature to be used in the TORT calculation.

INTERP next constructs arrays which describe the relationship between the large quadrature and the DOT quadrature. Arrays describing the characteristics of the large and small quadratures are also constructed. The quantity and level number of large quadrature eta levels overlapped by each small quadrature eta level are calculated and saved in an array. Similarly, the quantity, direction numbers, and fractions of large quadrature directions in an eta level overlapped by a given small quadrature direction are calculated and stored in an array. Coordinate system rotation is not accounted for in the calculation of these arrays. These arrays are calculated once for use later in the subroutine.

The boundary directional fluxes for each energy group are calculated separately and written to the output file before the calculation for the next group begins. Within the group loop, the 2-D DOT fluxes are read from the VISTA file. The large quadrature representation of the DOT fluxes is reduced to the small 3-D quadrature representation by using the previously calculated quadrature boundary arrays. These reduced fluxes are located at the 2-D mesh midpoints and have not been rotated. Next, a separate I-, J-, and K-boundary loop is used to calculate the fluxes on the respective 3-D region surfaces. Only the I-boundary loop will be described since each I-, J-, and K-boundary loop performs similar calculations.

The I-boundary calculation begins with a loop over all directions. A particular direction is directed inward on only one of the two I surfaces. The X-component of the 3-D spatial point is set equal to the X-component of the inward-directed surface.

Next are loops over all values of J and K. Now that the coordinates (I, J, K, MT) of the 3-D mesh point are known, the four neighboring 2-D mesh point positions

are determined. The unique rotation angle, α , for the 3-D point is calculated from the X and Y coordinates. The given small quadrature direction, MT, is rotated by the angle α to determine which small quadrature directions are overlapped. The fractions of the overlapped directions are calculated next. The fractions are used with the 2-D reduced fluxes (AFR) to calculate the reduced and rotated fluxes at the four neighboring 2-D mesh points. Two-dimensional linear interpolation between the four neighboring 2-D points is used to calculate the angular flux value for the 3-D mesh point.

After all I-, J-, and K-boundary directional fluxes have been calculated, they are written to a file in TORT boundary source file format.⁹ The group loop calculations are performed until the fluxes for all groups have been calculated and written to the output file.

Commons: **BIG**

Called from: **GETDAT**

Routines called: **WOT10, SEQIO, WRFLX, WOT4**

Argument list: (**TSEG, R1, Z1, AF, FIO, FJO, FKO, AWT, AMU, AETA, AXI, MMTADJ, MMTCOR, MNLVL, DDETA, DPHI, AWTS, AMUS, AETAS, AXIS, MNLVLS, DDETAS, DPHIS, NETAOV, METAOV, NMTETA, MTOVL, FOVL, AW0, LA, NETA2, NETAS, MTE1, DETA, MMT2, MMTS2, MMTOPP, MMTOPS, AFR, MMTAJS, PHIT1, PHIT2, MTE1S, DEAWTS**)

Arguments supplied:

TSEG - array containing the TORT x, y, and z mesh boundaries

R1 - array of DOT radial interval midpoints

Z1 - array of DOT axial interval midpoints

AWT - array of weights for large TORT quadrature

AMU - array of mu's for large TORT quadrature

AETA - array of eta's for large TORT quadrature

AWTS - array of weights for small TORT quadrature

AMUS - array of mu's for small TORT quadrature

AETAS - array of eta's for small TORT quadrature

AW0 - array containing DOT quadrature

NETA2 - half the number of eta levels in the large TORT quadrature

NETAS - number of eta levels in the small TORT quadrature

MMT2 - half the number of directions in the large TORT quadrature

MMTS2 - half the number of directions in the small TORT quadrature

Arguments modified:

AF - array of DOT fluxes from VISTA file

FIO - array of I-boundary directional fluxes

FJO - array of J-boundary directional fluxes

FKO - array of K-boundary directional fluxes

AXI - array of xi's for the large TORT quadrature

MMTADJ - array in table form providing the direction adjacent to a given TORT direction (large-quadrature)

MMTCOR - array in table form providing the DOT direction corresponding to a given TORT direction (large quadrature)

MNLVL - array in table form providing the eta level for a given TORT direction (large quadrature)

DDETA - array of eta increments for the large TORT quadrature

DPHI - array of azimuthal angle increments for the large TORT quadrature

AXIS - array of xi's for the small TORT quadrature

MNLVLS - array in table form providing the eta level for a given TORT direction (small quadrature)

- DDETAS - array of eta increments for the small quadrature
- DPHIS - array of azimuthal angle increments for the small quadrature
- NETAOV - number of large quadrature eta levels overlapped by a given direction in the small TORT quadrature
- METAOV - large quadrature eta levels overlapped by a given direction in the small TORT quadrature
- NMTETA - number of directions in a large quadrature eta level overlapped by a given small quadrature direction
- MTOVL - directions in a large quadrature eta level overlapped by a given small quadrature direction
- FOVL - fraction of a direction in a large quadrature eta level overlapped by a given small quadrature direction
- LA - large container array
- MTE1 - first non-zero weight direction in a large quadrature eta level
- DETA - array of eta level boundaries for large quadrature
- MMTOPP - opposite direction within an eta level for a given large quadrature direction
- MMTOPS - opposite direction within an eta level for a given small quadrature direction

AFR - array of DOT fluxes in reduced (small) quadrature representation

MMTAJS - array in table form providing the direction adjacent to a given direction (small quadrature)

PHIT1 - array of clockwise-most azimuthal angle boundaries (small quadrature)

PHIT2 - array of counterclockwise-most azimuthal angle boundaries (small quadrature)

MTE1S - array providing the first non-zero weight direction in an eta level (small quadrature)

DEAWTS - not used

COMMON BIG

Common block BIG is made up of several sets of variables. The first set of variables is an array of pointers for the container array LA and common block BIG. These pointers are in locations 3 through 47. The next set of variables in locations 48 and 49 are the logical unit numbers for input and output. Locations 50 through 67 contain alphanumeric data representing the title for a particular set of input data. VISTA alphanumeric and integer output data are stored in locations 68 through 108. Locations 109 through 113 contain information used for dimensioning subarrays within the container array LA. Data from the 1\$\$ input array are stored in locations 114 through 119. This integer information includes the number of intervals in the TORT mesh, the number of angles in the reduced quadrature set, and the logical unit numbers

for the VISTA input and DOTTOR output. The last set of variables in locations 120 through 122 is the 2** input array. This real array describes the position of the TORT mesh in the DOT mesh. Tables A.1 and A.2 show the contents of each location in common block BIG.

ADDITIONAL SUBROUTINES REQUIRED

The FORTRAN and assembler routines listed in Table A.3 are required in addition to the main program, GETDAT, and INTERP.

Table A.1. Array Pointers, Corresponding Arrays, and Array Lengths for Common BIG

Pointer Position	Array Pointer	Mnemonic Array Name	Array Length(words)
1	A(1)	Dummy variable	1
2	LIMA	Dummy variable	1
3	LNAXS	NXT (1\$\$ array)	6
4	LDEL	DELR (2** array)	3
5	LTSEG	TSEG (3** array)	NXT+NYT+NZT+3
6	LIVAL	Not used	NRD
7	LAW0	AW0	3*MM
8	LR1	R1	NRD
9	LZ1	Z1	NZD
10	LAF	AF	NRD*NZD*MM
11	LFIO	FIO	NYT*NZT*MMTS
12	LFJO	FJO	NXT*NZT*MMTS
13	LFKO	FKO	NXT*NYT*MMTS
14	LAWT	AWT	MMT
15	LAMU	AMU	MMT
16	LAETA	AETA	MMT
17	LAXI	AXI	MMT
18	LAWTS	AWTS (16** array)	MMTS
19	LAMUS	AMUS (17** array)	MMTS
20	LAETAS	AETAS (18** array)	MMTS
21	LAXIS	AXIS	MMTS
22	LAFR	AFR	NRD*NZD*MMTS
23	LMMTAJ	MMTADJ	MMT2
24	LMMTCO	MMTCOR	MMT
25	LMNLVL	MNLVL	MMT4
26	LDDETA	DDETA	NETA2
27	LDETA	DETA	NETA21
28	LMTE1	MTE1	NETA2
29	LDPHI	DPHI	MMT2
30	LMLVLS	MNLVLS	MMTS4
31	LDDETS	DDETAS	NETAS4
32	LDPHIS	DPHIS	MMTS4
33	LMTAJS	MMTAJS	MMTS
34	LPHIT1	PHIT1	MMTS
35	LPHIT2	PHIT2	MMTS
36	LMTE1S	MTE1S	NETAS
37	LDEWTS	DEAWTS	MMTS
38	LNETAO	NETAOV	MMTS
39	LMETAO	METAOV	MMTS*NETA2
40	LNMTET	NMTETA	MMTS*NETA2*MNMTET
41	LMTOVL	MTOVL	MMTS*NETA2*MNMTET
42	LFOVL	FOVL	MMTS*NETA2*MNMTET
43	LMTOPP	MTOPP	MMT2
44	LMTOPS	MTOPPS	MMTS4
45	LENER	ENER (not used)	IG+2
46	LSCRTC	I/O scratch space	NXT+NYT+NZT+IG+13
47	LAEND	LAEND	1

Table A.2. Layout and Description of Variables in Common BIG

Position	Variable	Description
48	NIN	Standard input unit (5)
49	NOU	Standard output unit (6)
50-67	TITLE(18)	Descriptive title
68-85	TDOT(18)	Not used by DOTTOR
86	MM	Number of directions in DOT quadrature
87-88	--	Not used by DOTTOR
89	IG	Number of energy groups
90-91	--	Not used by DOTTOR
92	NZD	Number of axial positions on VISTA output file
93-94	--	Not used by DOTTOR
95	NRD	Number of radial positions on VISTA output file
96-108	--	Not used by DOTTOR
109	MMT	Number of directions in large quadrature (2^*MM)
110	NETA	Number of eta levels in DOT quadrature
111	MNOVL	Estimate of maximum number of overlapped directions in a large quadrature eta level
112	MNETAO	Estimate of maximum number of large quadrature eta levels overlapped by a small quadrature eta level
113	MNMTE	Estimate of maximum number of large quadrature directions in an eta level overlapped by a small quadrature direction
114	NXT	Number of X spatial intervals (TORT)
115	NYT	Number of Y spatial intervals (TORT)
116	NZT	Number of Z spatial intervals (TORT)
117	MMTS	Number of directions in small 3-D quadrature
118	NVISA	Logical unit number of VISTA output file
119	NTAPE	Logical unit number of DOTOR output file
120	DELR	Radial position of TORT origin in DOT mesh
121	DELA	Angle from DOT radial axis to TORT X-axis
122	DELZ	Axial position of TORT origin in DOT mesh

Table A.3. Additional Subroutines Required by DOTTOR

Subroutine Name	Function	Subroutines Called
ALOCAF	FORTRAN version of ALOCAT	none
ALOCAT	Allocates and deallocates storage space (assembler routine)	none
BCDPRT	Machine-independent byte string printer	none
BUFIO	Reads/writes multiple arrays from buffer space	CLEARX,CMOVX,SEQIO,SKPEDV
CLEARX	Zeroes certain locations in an array	none
CLOSDA	Closes a FORTRAN direct access dataset (assembler routine)	none
CMOVX	Moves a block of data from one location to another	none
COMFIX	Initializes values in COMMON COMIN	none
CREN	Sets up parameters for the I/O package	none
DEFILE	Issues a define file with variable parameters (assembler routine)	none
DLOCAF	Passes words of storage to subroutine GETDAT	GETDAT
DLOCAL	Used with ALOCAT to allocate and deallocate storage	ALOCAT
DOPC	Opens and closes direct access datasets	CLEARX,CLOSDA,CREN,DEFILE, DLOCAL
DREN	Sets up parameters for the I/O package	none
EDIT	Machine-independent edit of irregular 2-D array	none
ERRO	Provides a diagnostic edit and (optional) dump	BCDPRT,ERRTRA,SKPEDI,SKPEDZ
ERRTRA	Provides error traceback	none

Table A.3 (continued)

Subroutine Name	Function	Subroutines Called
ERRSET	Modifies the FORTRAN error handling option table	none
FBSAM	Returns disk track capacity	KBLCK
FFREAD	Translates free/fixed format card images	none
FIDAS	Machine-independent input array processor	FFREAD
FIDOS	Linkage to FIDAS input processor	ERRO,FIDAS
HEADER	Prints a header message	none
KBLCK	Gets number of blocks per track (assembler routine)	none
REED	Performs sequential read from data files	CLEARX,ERRSET,SKPEDV
RITE	Performs sequential write to data files	CLEARX,ERRSET,SKPEDV
SEQIO	Provides sequential I/O control using subroutines REED and RITE	CLEARX,ERRO,REED,RITE
SKPEDI	Edits an array in I format with title and skips	BCDPRT
SKPEDZ	Edits an array in Z format with title and skips	BCDPRT
TIMEF	Provides job identification and timing information	ITIME,INTBCD
WOT4	Editing of 1-, 2-, 3-, or 4-D arrays with titles	BCDPRT,EDIT
WOT10	Prints 10 or less columns of irregular length	none
WRFLX	Writes 3-D flux output file	BUFI0,CMOVX,SEQIO,TIMEF

APPENDIX B

INPUT DATA DESCRIPTION

The first input variable, TITLE, is read in fixed format. The remaining input data are in the FIDO free-form format and are read by calls to the FIDOS routine.

Certain restrictions apply to some of the input data. The entire three-dimensional spatial mesh should be located inside the two-dimensional spatial mesh. Points outside the two-dimensional mesh will be set equal to the value of the nearest two-dimensional mesh point. Both the two-dimensional and the three-dimensional quadratures must be level symmetric. "Level symmetric" means that the angles subtended by the latitudinal level lines remain constant as the mu's are varied.⁴ The number of directions, MMTS, in the three-dimensional quadrature must be less than or equal to twice the number of directions, MM, in the two-dimensional quadrature.

Fixed format:

TITLE(I),I=1,18	---	FORMAT (18A4)
72 character title describing problem or		
input data		

FIDO free-form

1\$\$	(1) NXT	---	number of x spatial intervals (TORT)
	(2) NYT	---	number of y spatial intervals (TORT)
	(3) NZT	---	number of z spatial intervals (TORT)
	(4) MMTS	---	number of directions in reduced quadrature (MMTS .LE. 2*MM)

	(5) NVISA	---	logical unit number of VISTA code flux input (default = 20)
	(6) NTAPE	---	logical unit number of DOTTOR boundary directional output (default = 21)
	T		terminate block
2**	(1) DELR	---	radial distance from DOT origin to TORT origin
	(2) DELA	---	angle (radians) measured counterclockwise from DOT radial axis to TORT x-axis (0.0 .LE. DELA .LE. 2*PI)
	(3) DELZ	---	axial distance from DOT origin to TORT origin
	T		terminate block
3**	TSEG	---	TORT mesh boundaries (x, then y, then z) (TSEG(I),I=1,NXT+XYT+NZT+3)
16**	AWTS	---	weight values for small TORT quadrature (AWTS(I),I=1,MMTS)
17**	AMUS	---	mu values for small TORT quadrature (AMUS(I),I=1,MMTS)
18**	AETAS	---	eta values for small TORT quadrature (AETAS(I),I=1,MMTS)
	T		terminate block

APPENDIX C

SAMPLE PROBLEM INPUT AND OUTPUT

This sample problem is an example of the use of the DOTTOR code. The DOT calculation is an R-Z geometry air-over-ground problem with the source located at $R=0$, $Z=30,000$ cm. An S6 quadrature was used with the air/ground interface at $Z=0$. For this example, the results of the DOT and VISTA calculations are assumed to be available. The output file from the VISTA code is available on logical unit 20.

A 3-D discrete ordinates (TORT) calculation is desired in a $5 \times 3 \times 3$ region located radially at $\Delta R = 700$ cm, axially at $\Delta Z = 30$ cm, and rotated $\alpha = 73^\circ$. The mesh boundaries for the $5 \times 3 \times 3$ region extend from -155.0 cm to 155.0 cm in the X direction, -55.0 cm to 55.0 cm in the Y direction, and -10.0 cm to 110.0 cm in the Z direction. The DOT S6 quadrature is reduced by DOTTOR to an S2 quadrature for use by TORT. Sample DOTTOR input for this example is shown in Fig. C.1.

The DOTTOR output (see Fig. C.2) begins by printing the problem description provided as input data. This is followed by the 1\$\$ array, the 2** array, and the integer data read from the VISTA file. Next, the number of words of storage required by the problem versus the number of words of storage available are provided for user convenience. Printed next are the DOT mesh midpoints and the TORT mesh boundaries followed by the large and small TORT quadrature sets. The next seventeen arrays printed, beginning with MMTADJ and ending with FOVL, are used mainly for troubleshooting and code debugging. The arrays are defined in the description of subroutine INTERP in Appendix A. These arrays are followed by the position of the DOT Z-axis in the TORT X-Y plane, XBARD and YBARD.

SAMPLE PROBLEM, 5X3X3, S6-S2
1\$\$ 5 3 3 12 20 30 T
2** 700.0 1.27409 0.0 T
3** -155 -150 -50 M3 /I-BOUNDARIES
-55 -50 M2 /J-BOUNDARIES
-10 0 100 110 /K-BOUNDARIES
/ S2 FULL SYM -- 12 DIRECTIONS
16** 0 2R.125 3QJ
17** -.8165 -.57735 M1 Q3 Q6
18** 6R-.57735 G6
T

Fig. C.1. DOTTOR sample problem input

```

SAMPLE PROBLEM, 5X3X3, S6-S2
1$ ARRAY   6 ENTRIES READ
 0T
2* ARRAY   3 ENTRIES READ
 0T
1 1$$
NXT      =      5          NUMBER OF TORT X-AXIS SEGMENTS
NYT      =      3          NUMBER OF TORT Y-AXIS SEGMENTS
NZT      =      3          NUMBER OF TORT Z-AXIS SEGMENTS
MMTS     =     12         NUMBER OF DIRECTIONS IN TORT SMALL QUADRATURE
NVISA    =     20         UNIT NUMBER OF INPUT FROM VISA
NTAPE    =     30         UNIT NUMBER OF DOTTOR OUTPUT

2**
DELR     =  0.700000E+03 RADIAL POSITION OF TORT ORIGIN IN DOT MESH
DELA     =  0.127409E+01 ANGLE (RADIAN) BETWEEN DOT RADIAL AXIS AND TORT X-AXIS
DELZ     =      0.0        AXIAL POSITION OF TORT ORIGIN IN DOT MESH

----- INPUT FROM VISA TAPE -----
TITLE     =  VISA TEST FOR DOTTOR
TDOT      =  "DOT AIR / GROUND PROBLEM
MM        =      30
IM        =      48
JM        =      57
IG        =      2
IGP       =      3
MMDN     =      15
NZD/NJP  =      10
SH        =      0.0
HSA       =      0.0
NRD/NIP  =      6
JPL       =      15
JPU       =      24
NED       =      0
ISKP      =      0
ISGRP     =      0
NFLSV    =      16
NAFT     =      15
NUNCL    =      14
NDATA    =      20
N5        =      5
N6        =      6
NJ1       =      1
NJM      =      57

/ S2 FULL SYM -- 12 DIRECTIONS
3* ARRAY           14 ENTRIES READ
16* ARRAY          12 ENTRIES READ
17* ARRAY          12 ENTRIES READ
18* ARRAY          12 ENTRIES READ
 0T

```

WORDS STORAGE AVAILABLE	101376
WORDS STORAGE REQUIRED	4060

Fig. C.2. DOTTOR sample problem output

DOT MESH POINTS			TORT MESH BOUNDARIES		
	R	Z	X	Y	Z
1	2.00000E+02	-3.50000E+01	-1.55000E+02	-5.50000E+01	-1.00000E+01
2	3.00000E+02	-2.50000E+01	-1.50000E+02	-5.00000E+01	0.0
3	4.00000E+02	-1.50000E+01	-5.00000E+01	5.00000E+01	1.00000E+02
4	5.48333E+02	-5.00000E+00	5.00000E+01	5.50000E+01	1.10000E+02
5	7.45000E+02	5.00000E+01	1.50000E+02		
6	9.41667E+02	1.50000E+02	1.55000E+02		
7		2.50000E+02			
8		3.50000E+02			
9		4.50000E+02			
10		5.50000E+02			
LARGE TORT QUADRATURE					
M	WEIGHT	MU	XI	ETA	WEIGHT
1	0.0	-3.65150E-01	0.0	-9.30950E-01	0.0
2	2.08335E-02	-2.58200E-01	-2.58196E-01	-9.30950E-01	1.25000E-01
3	2.08335E-02	2.58200E-01	-2.58196E-01	-9.30950E-01	1.25000E-01
4	0.0	-7.30300E-01	0.0	-6.83130E-01	0.0
5	2.08335E-02	-6.83130E-01	-2.58199E-01	-6.83130E-01	1.25000E-01
6	2.08335E-02	-2.58200E-01	-6.83130E-01	-6.83130E-01	1.25000E-01
7	2.08335E-02	2.58200E-01	-6.83130E-01	-6.83130E-01	1.25000E-01
8	2.08335E-02	6.83130E-01	-2.58199E-01	-6.83130E-01	1.25000E-01
9	0.0	-9.66090E-01	0.0	-2.58200E-01	1.25000E-01
10	2.08335E-02	-9.30950E-01	-2.58196E-01	-2.58200E-01	0.0
11	2.08335E-02	-6.83130E-01	-6.83130E-01	-2.58200E-01	1.25000E-01
12	2.08335E-02	-2.58200E-01	-9.30949E-01	-2.58200E-01	1.25000E-01
13	2.08335E-02	2.58200E-01	-9.30949E-01	-2.58200E-01	
14	2.08335E-02	6.83130E-01	-6.83130E-01	-2.58200E-01	
15	2.08335E-02	9.30950E-01	-2.58196E-01	-2.58200E-01	
16	0.0	-3.65150E-01	0.0	-9.30950E-01	
17	2.08335E-02	-2.58200E-01	2.58196E-01	-9.30950E-01	
18	2.08335E-02	2.58200E-01	2.58196E-01	-9.30950E-01	
19	0.0	-7.30300E-01	0.0	-6.83130E-01	
20	2.08335E-02	-6.83130E-01	2.58199E-01	-6.83130E-01	
21	2.08335E-02	-2.58200E-01	6.83130E-01	-6.83130E-01	
22	2.08335E-02	2.58200E-01	6.83130E-01	-6.83130E-01	
23	2.08335E-02	6.83130E-01	2.58199E-01	-6.83130E-01	
24	0.0	-9.66090E-01	0.0	-2.58200E-01	
25	2.08335E-02	-9.30950E-01	2.58196E-01	-2.58200E-01	
26	2.08335E-02	-6.83130E-01	6.83130E-01	-2.58200E-01	
27	2.08335E-02	-2.58200E-01	9.30949E-01	-2.58200E-01	
28	2.08335E-02	2.58200E-01	9.30949E-01	-2.58200E-01	
29	2.08335E-02	6.83130E-01	6.83130E-01	-2.58200E-01	
30	2.08335E-02	9.30950E-01	2.58196E-01	-2.58200E-01	
31	0.0	-3.65150E-01	0.0	9.30950E-01	
32	2.08335E-02	-2.58200E-01	-2.58196E-01	9.30950E-01	
33	2.08335E-02	2.58200E-01	-2.58196E-01	9.30950E-01	
34	0.0	-7.30300E-01	0.0	6.83130E-01	
35	2.08335E-02	-6.83130E-01	-2.58199E-01	6.83130E-01	
36	2.08335E-02	-2.58200E-01	-6.83130E-01	6.83130E-01	
37	2.08335E-02	2.58200E-01	-6.83130E-01	6.83130E-01	
38	2.08335E-02	6.83130E-01	-2.58199E-01	6.83130E-01	
39	0.0	-9.66090E-01	0.0	2.58200E-01	
40	2.08335E-02	-9.30950E-01	-2.58196E-01	2.58200E-01	

Fig. C.2 (continued)

41	2.08335E-02	-6.83130E-01	-6.83130E-01	2.58200E-01
42	2.08335E-02	-2.58200E-01	-9.30949E-01	2.58200E-01
43	2.08335E-02	2.58200E-01	-9.30949E-01	2.58200E-01
44	2.08335E-02	6.83130E-01	-6.83130E-01	2.58200E-01
45	2.08335E-02	9.30950E-01	-2.58196E-01	2.58200E-01
46	0.0	-3.65150E-01	0.0	9.30950E-01
47	2.08335E-02	-2.58200E-01	2.58196E-01	9.30950E-01
48	2.08335E-02	2.58200E-01	2.58196E-01	9.30950E-01
49	0.0	-7.30300E-01	0.0	6.83130E-01
50	2.08335E-02	-6.83130E-01	2.58199E-01	6.83130E-01
51	2.08335E-02	-2.58200E-01	6.83130E-01	6.83130E-01
52	2.08335E-02	2.58200E-01	6.83130E-01	6.83130E-01
53	2.08335E-02	6.83130E-01	2.58199E-01	6.83130E-01
54	0.0	-9.66090E-01	0.0	2.58200E-01
55	2.08335E-02	-9.30950E-01	2.58196E-01	2.58200E-01
56	2.08335E-02	-6.83130E-01	6.83130E-01	2.58200E-01
57	2.08335E-02	-2.58200E-01	9.30949E-01	2.58200E-01
58	2.08335E-02	2.58200E-01	9.30949E-01	2.58200E-01
59	2.08335E-02	6.83130E-01	6.83130E-01	2.58200E-01
60	2.08335E-02	9.30950E-01	2.58196E-01	2.58200E-01

Fig. C.2 (continued)

M	MMTADJ	MMTCOR	MNLVL	DPHI	MNLVLS	DPHIS
1	1	1	1	0.0	1	0.0
2	3	2	1	1.57080E+00	1	1.57080E+00
3	18	3	1	1.57080E+00	1	1.57080E+00
4	4	4	2	0.0	1	0.0
5	6	5	2	7.85399E-01	1	1.57080E+00
6	7	6	2	7.85399E-01	1	1.57080E+00
7	8	7	2	7.85399E-01	2	0.0
8	23	8	2	7.85399E-01	2	1.57080E+00
9	9	9	3	0.0	2	1.57080E+00
10	11	10	3	5.23600E-01	2	0.0
11	12	11	3	5.23600E-01	2	1.57080E+00
12	13	12	3	5.23600E-01	2	1.57080E+00
13	14	13	3	5.23600E-01		
14	15	14	3	5.23600E-01		
15	30	15	3	5.23600E-01		
16	16	1		0.0		
17	2	2		1.57080E+00		
18	17	3		1.57080E+00		
19	19	4		0.0		
20	5	5		7.85399E-01		
21	20	6		7.85399E-01		
22	21	7		7.85399E-01		
23	22	8		7.85399E-01		
24	24	9		0.0		
25	10	10		5.23600E-01		
26	25	11		5.23600E-01		
27	26	12		5.23600E-01		
28	27	13		5.23600E-01		
29	28	14		5.23600E-01		
30	29	15		5.23600E-01		
31		16				
32		17				
33		18				
34		19				
35		20				
36		21				
37		22				
38		23				
39		24				
40		25				
41		26				
42		27				
43		28				
44		29				

Fig. C.2 (continued)

45	30
46	16
47	17
48	18
49	19
50	20
51	21
52	22
53	23
54	24
55	25
56	26
57	27
58	28
59	29
60	30

M	MMTAJS	PHIT1	PHIT2	MTE1S
1	1	0.0	0.0	2
2	3	0.0	1.57080E+00	8
3	6	1.57080E+00	3.14159E+00	
4	4	0.0	0.0	
5	2	4.71239E+00	6.28318E+00	
6	5	3.14159E+00	4.71239E+00	
7	0	0.0	0.0	
8	9	0.0	1.57080E+00	
9	12	1.57080E+00	3.14159E+00	
10	0	0.0	0.0	
11	8	4.71239E+00	6.28318E+00	
12	11	3.14159E+00	4.71239E+00	

MTS	NETAOV	METAOV	NMTETA	MTOVL	FOVL
1	0	0	0	1	0.0
2	3	1	1	2	1.000000
2	3	2	2	5	1.000000
2	3	2	2	6	1.000000
2	3	3	3	10	1.000000
2	3	3	3	11	1.000000
2	3	3	3	12	1.000000
3	3	1	2	2	0.0
3	3	1	2	3	1.000000
3	3	2	3	6	0.0
3	3	2	3	7	1.000000
3	3	2	3	8	1.000000
3	3	3	4	12	0.0
3	3	3	4	13	1.000000

Fig. C.2 (continued)

3	3	3	4	14	1.000000
3	3	3	4	15	1.000000
4	0	0	0	0	0.0
5	3	1	2	18	0.0
5	3	1	2	17	1.000000
5	3	2	3	22	0.0
5	3	2	3	21	1.000000
5	3	2	3	20	1.000000
5	3	3	4	28	0.0
5	3	3	4	27	1.000000
5	3	3	4	26	1.000000
5	3	3	4	25	1.000000
6	3	1	1	18	1.000000
6	3	2	2	23	1.000000
6	3	2	2	22	1.000000
6	3	3	3	30	1.000000
6	3	3	3	29	1.000000
6	3	3	3	28	1.000000
7	0	3	0	31	0.0
8	3	4	1	32	1.000000
8	3	5	2	35	1.000000
8	3	5	2	36	1.000000
8	3	6	3	40	1.000000
8	3	6	3	41	1.000000
8	3	6	3	42	1.000000
9	3	4	2	32	0.0
9	3	4	2	33	1.000000
9	3	5	3	36	0.0
9	3	5	3	37	1.000000
9	3	5	3	38	1.000000
9	3	6	4	42	0.0
9	3	6	4	43	1.000000
9	3	6	4	44	1.000000
9	3	6	4	45	1.000000
10	0	3	0	30	0.0
11	3	4	2	48	0.0
11	3	4	2	47	1.000000
11	3	5	3	52	0.0
11	3	5	3	51	1.000000
11	3	5	3	50	1.000000
11	3	6	4	58	0.0
11	3	6	4	57	1.000000
11	3	6	4	56	1.000000
11	3	6	4	55	1.000000
12	3	4	1	48	1.000000
12	3	5	2	53	1.000000
12	3	5	2	52	1.000000
12	3	6	3	60	1.000000
12	3	6	3	59	1.000000
12	3	6	3	58	1.000000

Fig. C.2 (continued)

XBAR = -0.20466037E=03
YBAR = 0.66941260E=03

0GROUP =	1
0IGG,MM,I,J,K,LAST 5 FKO	1 12 5 3 3 4.814406E-14 9.900208E-14 0
0GROUP =	2
0IGG,MM,I,J,K,LAST 5 FKO	2 12 5 3 3 3.412400E-14 7.092086E-14 0

0AF

0Z

				1		
0 M	R 1	R 2	R 3	R 4	R 5	R 6
1	6.30280E-13	6.21371E-13	6.13436E-13	6.06297E-13	5.94112E-13	5.82785E-13
2	8.12919E-13	8.00384E-13	7.88122E-13	7.76476E-13	7.56472E-13	7.38448E-13
3	8.45286E-13	8.46113E-13	8.46680E-13	8.49903E-13	8.52017E-13	8.53001E-13
4	3.17521E-14	3.13706E-14	3.09994E-14	3.06524E-14	3.00736E-14	2.95393E-14
5	3.35157E-14	3.31403E-14	3.27684E-14	3.24165E-14	3.18238E-14	3.12716E-14
6	3.40828E-14	3.39878E-14	3.39033E-14	3.38345E-14	3.36701E-14	3.35405E-14
7	3.45354E-14	3.46421E-14	3.47365E-14	3.48950E-14	3.50459E-14	3.52032E-14
8	3.68200E-14	3.51767E-14	3.52977E-14	3.56395E-14	3.59557E-14	3.62957E-14
9	9.83182E-17	7.88112E-17	4.39849E-17	1.70021E-17	1.31800E-17	6.12903E-18
10	1.43344E-16	1.08927E-16	6.18067E-17	2.33692E-17	1.77765E-17	8.72749E-18
11	1.14165E-16	8.17654E-17	4.60969E-17	1.67572E-17	1.24081E-17	6.32720E-18
12	5.09560E-17	2.88475E-17	1.51188E-17	4.97951E-18	3.16172E-18	1.66121E-18
13	5.50153E-17	2.46521E-17	1.62242E-17	5.41810E-18	2.93621E-18	2.11901E-18
14	1.78598E-16	7.76472E-17	6.05789E-17	2.29806E-17	1.27858E-17	1.07266E-17
15	3.04982E-16	1.20430E-16	9.22037E-17	3.72883E-17	2.02439E-17	1.74960E-17
16	0.0	0.0	0.0	0.0	0.0	0.0

17 THROUGH 30 SAME AS ABOVE

0Z

				2		
0 M	R 1	R 2	R 3	R 4	R 5	R 6
1	2.09486E-12	2.06495E-12	2.03836E-12	2.01451E-12	1.97391E-12	1.93623E-12
2	2.70129E-12	2.65950E-12	2.61862E-12	2.57980E-12	2.51317E-12	2.45318E-12
3	2.80906E-12	2.81154E-12	2.81332E-12	2.82397E-12	2.83086E-12	2.83398E-12
4	2.05855E-13	2.03327E-13	2.00869E-13	1.98555E-13	1.94753E-13	1.91268E-13
5	2.17187E-13	2.14718E-13	2.12266E-13	2.09928E-13	2.06046E-13	2.02445E-13
6	2.20641E-13	2.20023E-13	2.19473E-13	2.19003E-13	2.17914E-13	2.17055E-13
7	2.23577E-13	2.24278E-13	2.24858E-13	2.25845E-13	2.26805E-13	2.27809E-13
8	2.30111E-13	2.27015E-13	2.28535E-13	2.30628E-13	2.32656E-13	2.34870E-13
9	2.50307E-15	2.43279E-15	1.71820E-15	7.70204E-16	7.44006E-16	4.78418E-16
10	3.29971E-15	2.94998E-15	2.12582E-15	9.72312E-16	8.86570E-16	5.94082E-16
11	2.84149E-15	2.37711E-15	1.72403E-15	7.86702E-16	6.82601E-16	4.72833E-16
12	1.58392E-15	1.09225E-15	7.60198E-16	3.41566E-16	2.56611E-16	1.81276E-16
13	1.48966E-15	9.37955E-16	7.37419E-16	3.27983E-16	2.32045E-16	1.92107E-16
14	2.98029E-15	1.94245E-15	1.81967E-15	8.14097E-16	6.09345E-16	5.79902E-16
15	3.99631E-15	2.42424E-15	2.42311E-15	1.09004E-15	8.06264E-16	8.13377E-16
16	0.0	0.0	0.0	0.0	0.0	0.0

17 THROUGH 30 SAME AS ABOVE

Fig. C.2 (continued)

OZ	3	R 1	R 2	R 3	R 4	R 5	R 6
0 M							
1	6.96277E-12	6.86229E-12	6.77321E-12	6.69355E-12	6.55829E-12	6.43288E-12	
2	8.97629E-12	8.83693E-12	8.70067E-12	8.57131E-12	8.34939E-12	8.14968E-12	
3	9.33503E-12	9.34245E-12	9.34798E-12	9.38321E-12	9.40570E-12	9.41553E-12	
4	1.33469E-12	1.31792E-12	1.30172E-12	1.28622E-12	1.26122E-12	1.23848E-12	
5	1.40747E-12	1.39122E-12	1.37511E-12	1.35954E-12	1.33408E-12	1.31061E-12	
6	1.42817E-12	1.42424E-12	1.42069E-12	1.41755E-12	1.41034E-12	1.40465E-12	
7	1.44755E-12	1.45202E-12	1.45556E-12	1.46169E-12	1.46781E-12	1.47421E-12	
8	1.45941E-12	1.47036E-12	1.47946E-12	1.49237E-12	1.50543E-12	1.51986E-12	
9	6.26950E-14	6.22472E-14	6.00014E-14	3.45528E-14	3.38573E-14	3.24416E-14	
10	7.36348E-14	6.95363E-14	6.55611E-14	3.96172E-14	3.75716E-14	3.54507E-14	
11	6.88075E-14	6.26397E-14	5.81944E-14	3.61473E-14	3.34067E-14	3.12640E-14	
12	5.05789E-14	4.18427E-14	3.68269E-14	2.38205E-14	2.05571E-14	1.85156E-14	
13	4.63047E-14	3.85827E-14	3.45695E-14	2.22659E-14	1.95026E-14	1.78915E-14	
14	6.08250E-14	5.64786E-14	5.51862E-14	3.35949E-14	3.22072E-14	3.16797E-14	
15	6.50773E-14	6.30898E-14	6.38831E-14	3.74161E-14	3.73366E-14	3.78471E-14	
16	0.0	0.0	0.0	0.0	0.0	0.0	
17 THROUGH 30 SAME AS ABOVE							
OZ	4	R 1	R 2	R 3	R 4	R 5	R 6
0 M							
1	2.31427E-11	2.28050E-11	2.25066E-11	2.22404E-11	2.17897E-11	2.13725E-11	
2	2.98279E-11	2.93632E-11	2.89091E-11	2.84779E-11	2.77386E-11	2.70739E-11	
3	3.10219E-11	3.10438E-11	3.10612E-11	3.11776E-11	3.12507E-11	3.12818E-11	
4	8.65459E-12	8.54279E-12	8.43673E-12	8.33232E-12	8.16788E-12	8.01940E-12	
5	9.12149E-12	9.01433E-12	8.90911E-12	8.80486E-12	8.63788E-12	8.48478E-12	
6	9.24285E-12	9.21855E-12	9.19607E-12	9.17516E-12	9.12765E-12	9.09011E-12	
7	9.37276E-12	9.40083E-12	9.42199E-12	9.46009E-12	9.49915E-12	9.54004E-12	
8	9.44917E-12	9.52073E-12	9.57711E-12	9.65662E-12	9.74096E-12	9.83523E-12	
9	1.57034E-12	1.55860E-12	1.54777E-12	1.55021E-12	1.51867E-12	1.48733E-12	
10	1.59588E-12	1.58770E-12	1.57880E-12	1.58394E-12	1.55715E-12	1.52942E-12	
11	1.60859E-12	1.60950E-12	1.60722E-12	1.61669E-12	1.60275E-12	1.58640E-12	
12	1.63492E-12	1.64145E-12	1.64434E-12	1.65498E-12	1.65471E-12	1.65266E-12	
13	1.65126E-12	1.66251E-12	1.67024E-12	1.68967E-12	1.69971E-12	1.70808E-12	
14	1.64614E-12	1.66172E-12	1.67258E-12	1.70575E-12	1.72296E-12	1.73843E-12	
15	1.64772E-12	1.66333E-12	1.67398E-12	1.71530E-12	1.73651E-12	1.75669E-12	
16	0.0	0.0	0.0	0.0	0.0	0.0	
17 THROUGH 30 SAME AS ABOVE							
OZ	5	R 1	R 2	R 3	R 4	R 5	R 6
0 M							
1	3.57890E-11	3.52473E-11	3.47702E-11	3.43499E-11	3.36448E-11	3.29962E-11	
2	4.61042E-11	4.53784E-11	4.46684E-11	4.39942E-11	4.28396E-11	4.18039E-11	
3	4.79650E-11	4.79817E-11	4.80071E-11	4.81845E-11	4.82876E-11	4.83264E-11	
4	1.50984E-11	1.49051E-11	1.47154E-11	1.45311E-11	1.42325E-11	1.39665E-11	
5	1.58845E-11	1.57065E-11	1.55251E-11	1.53485E-11	1.50484E-11	1.47749E-11	
6	1.61062E-11	1.60620E-11	1.60204E-11	1.59811E-11	1.58941E-11	1.58235E-11	
7	1.63314E-11	1.63740E-11	1.64036E-11	1.64667E-11	1.65340E-11	1.66045E-11	
8	1.64735E-11	1.65844E-11	1.66713E-11	1.68009E-11	1.69544E-11	1.71217E-11	
9	6.34978E-12	6.30280E-12	6.25472E-12	6.17590E-12	6.05915E-12	5.93438E-12	
10	6.49328E-12	6.44499E-12	6.39609E-12	6.31969E-12	6.21229E-12	6.09973E-12	
11	6.53100E-12	6.50798E-12	6.48138E-12	6.43941E-12	6.37850E-12	6.30904E-12	
12	6.57073E-12	6.55911E-12	6.55149E-12	6.54364E-12	6.53186E-12	6.51755E-12	
13	6.61759E-12	6.62847E-12	6.64280E-12	6.66796E-12	6.69682E-12	6.72267E-12	
14	6.65791E-12	6.69500E-12	6.72815E-12	6.77563E-12	6.83690E-12	6.89434E-12	
15	6.67604E-12	6.71970E-12	6.76243E-12	6.82436E-12	6.90565E-12	6.98479E-12	
16	0.0	0.0	0.0	0.0	0.0	0.0	
17 THROUGH 18 SAME AS ABOVE							

Fig. C.2 (continued)

19	1.12553E-15	9.86422E-16	8.57391E-16	6.63407E-16	4.16673E-16	1.51646E-16	
20	1.15327E-15	1.02489E-15	9.08515E-16	7.21866E-16	5.11249E-16	2.17130E-16	
21	1.33937E-15	1.31529E-15	1.27084E-15	1.23485E-15	1.16084E-15	1.10684E-15	
22	1.62337E-15	1.71753E-15	1.80704E-15	1.91661E-15	2.06064E-15	2.21302E-15	
23	1.82399E-15	2.00358E-15	2.18769E-15	2.42026E-15	2.72973E-15	3.03906E-15	
24	6.80351E-14	6.72970E-14	6.66282E-14	6.56411E-14	6.43838E-14	6.34069E-14	
25	6.81366E-14	6.74170E-14	6.67623E-14	6.57987E-14	6.45723E-14	6.36235E-14	
26	6.84215E-14	6.78384E-14	6.73292E-14	6.65533E-14	6.55299E-14	6.48349E-14	
27	6.90380E-14	6.87114E-14	6.84000E-14	6.80735E-14	6.74120E-14	6.71701E-14	
28	6.97888E-14	6.97823E-14	6.97413E-14	6.98332E-14	6.97556E-14	6.97404E-14	
29	7.04676E-14	7.07895E-14	7.10337E-14	7.13998E-14	7.18731E-14	7.22284E-14	
30	7.08997E-14	7.14069E-14	7.18248E-14	7.23893E-14	7.30914E-14	7.37315E-14	
OZ	6						
0 M		R 1	R 2	R 3	R 4	R 5	R 6
	1	3.62168E-11	3.56315E-11	3.51159E-11	3.46718E-11	3.39419E-11	3.32786E-11
	2	4.66054E-11	4.58575E-11	4.51247E-11	4.44282E-11	4.32380E-11	4.21750E-11
	3	4.85075E-11	4.84949E-11	4.85228E-11	4.86965E-11	4.87805E-11	4.88023E-11
	4	1.53018E-11	1.51233E-11	1.49288E-11	1.47297E-11	1.44032E-11	1.41164E-11
	5	1.60802E-11	1.59094E-11	1.57279E-11	1.55428E-11	1.52219E-11	1.49295E-11
	6	1.62950E-11	1.62431E-11	1.61963E-11	1.61525E-11	1.60585E-11	1.59775E-11
	7	1.65182E-11	1.65430E-11	1.65622E-11	1.66220E-11	1.66903E-11	1.67610E-11
	8	1.66616E-11	1.67546E-11	1.68194E-11	1.69503E-11	1.71187E-11	1.72910E-11
	9	6.41603E-12	6.37219E-12	6.32934E-12	6.26559E-12	6.17622E-12	6.06720E-12
	10	6.56533E-12	6.51863E-12	6.47261E-12	6.40413E-12	6.31045E-12	6.20729E-12
	11	6.60168E-12	6.57789E-12	6.55205E-12	6.51398E-12	6.46094E-12	6.39934E-12
	12	6.64032E-12	6.62658E-12	6.61710E-12	6.61048E-12	6.60146E-12	6.59015E-12
	13	6.68861E-12	6.69848E-12	6.70789E-12	6.73121E-12	6.75926E-12	6.78436E-12
	14	6.73017E-12	6.76707E-12	6.79928E-12	6.84738E-12	6.90920E-12	6.96196E-12
	15	6.74855E-12	6.79283E-12	6.83633E-12	6.90013E-12	6.98271E-12	7.05885E-12
	16	0.0	0.0	0.0	0.0	0.0	0.0
	17 THROUGH 18	SAME AS ABOVE					
	19	3.41980E-15	3.01276E-15	2.61806E-15	2.04726E-15	1.29541E-15	5.02660E-16
	20	3.52171E-15	3.14926E-15	2.76860E-15	2.25931E-15	1.55456E-15	7.23209E-16
	21	4.02208E-15	3.91797E-15	3.79760E-15	3.58634E-15	3.46666E-15	3.30695E-15
	22	4.86363E-15	5.16908E-15	5.44752E-15	5.79247E-15	6.23474E-15	6.71190E-15
	23	5.50907E-15	5.97153E-15	6.50995E-15	7.22959E-15	8.15935E-15	9.08377E-15
	24	2.17935E-13	2.10623E-13	2.01124E-13	1.93868E-13	1.90450E-13	1.87473E-13
	25	2.21704E-13	2.13944E-13	2.04318E-13	1.96198E-13	1.91547E-13	1.88242E-13
	26	2.14352E-13	2.08371E-13	2.02385E-13	1.97280E-13	1.94264E-13	1.91936E-13
	27	2.08440E-13	2.05607E-13	2.02664E-13	2.00489E-13	1.98894E-13	1.97973E-13
	28	2.08219E-13	2.07083E-13	2.05743E-13	2.06152E-13	2.06198E-13	2.06352E-13
	29	2.13661E-13	2.09425E-13	2.10412E-13	2.11304E-13	2.12858E-13	2.14105E-13
	30	2.26453E-13	2.19287E-13	2.19140E-13	2.18334E-13	2.17115E-13	2.18594E-13
OZ	7						
0 M		R 1	R 2	R 3	R 4	R 5	R 6
	1	3.66661E-11	3.60369E-11	3.54757E-11	3.50011E-11	3.42433E-11	3.35643E-11
	2	4.71164E-11	4.63464E-11	4.55903E-11	4.48703E-11	4.36427E-11	4.25508E-11
	3	4.90363E-11	4.90123E-11	4.90469E-11	4.92143E-11	4.92768E-11	4.92817E-11
	4	1.54873E-11	1.53259E-11	1.51477E-11	1.49438E-11	1.45913E-11	1.42744E-11
	5	1.62743E-11	1.61040E-11	1.59322E-11	1.57466E-11	1.54090E-11	1.50916E-11
	6	1.64857E-11	1.64194E-11	1.63647E-11	1.63183E-11	1.62226E-11	1.61331E-11
	7	1.66906E-11	1.67006E-11	1.67129E-11	1.67737E-11	1.68454E-11	1.69179E-11
	8	1.68319E-11	1.69009E-11	1.69596E-11	1.71079E-11	1.72913E-11	1.74591E-11
	9	6.47428E-12	6.42781E-12	6.38262E-12	6.31936E-12	6.24046E-12	6.16938E-12
	10	6.63306E-12	6.58441E-12	6.53672E-12	6.46887E-12	6.38178E-12	6.29702E-12
	11	6.67067E-12	6.64480E-12	6.61459E-12	6.57431E-12	6.52375E-12	6.46976E-12
	12	6.71114E-12	6.69641E-12	6.68289E-12	6.67036E-12	6.65859E-12	6.64798E-12
	13	6.75964E-12	6.76839E-12	6.78050E-12	6.79961E-12	6.82105E-12	6.83909E-12

Fig. C.2 (continued)

14	6.80248E-12	6.84020E-12	6.87582E-12	6.92467E-12	6.97883E-12	7.02110E-12	
15	6.82302E-12	6.86843E-12	6.91281E-12	6.97577E-12	7.05323E-12	7.12268E-12	
16	0.0	0.0	0.0	0.0	0.0	0.0	
17 THROUGH 18 SAME AS ABOVE							
19	5.79413E-15	5.12245E-15	4.46719E-15	3.52784E-15	2.22026E-15	1.02540E-15	
20	6.00932E-15	5.37411E-15	4.77375E-15	3.92510E-15	2.62118E-15	1.47084E-15	
21	6.77276E-15	6.58571E-15	6.41193E-15	6.13733E-15	5.74440E-15	5.46797E-15	
22	8.07024E-15	8.55835E-15	9.03054E-15	9.68717E-15	1.05203E-14	1.13267E-14	
23	9.22928E-15	9.91123E-15	1.07426E-14	1.19661E-14	1.35139E-14	1.50417E-14	
24	3.37310E-13	3.32101E-13	3.29972E-13	3.26600E-13	3.19304E-13	3.09460E-13	
25	3.40492E-13	3.35434E-13	3.33243E-13	3.29893E-13	3.22623E-13	3.11919E-13	
26	3.47069E-13	3.39265E-13	3.32086E-13	3.25746E-13	3.19702E-13	3.14345E-13	
27	3.48904E-13	3.39675E-13	3.32299E-13	3.27468E-13	3.24646E-13	3.22894E-13	
28	3.48502E-13	3.40509E-13	3.37064E-13	3.35394E-13	3.36311E-13	3.36559E-13	
29	3.55818E-13	3.48599E-13	3.47194E-13	3.47041E-13	3.47545E-13	3.50314E-13	
30	3.69492E-13	3.70313E-13	3.65637E-13	3.62069E-13	3.59333E-13	3.59543E-13	
OZ	8						
0 M		R 1	R 2	R 3	R 4	R 5	R 6
1	3.71357E-11	3.64657E-11	3.58540E-11	3.53388E-11	3.45494E-11	3.38536E-11	
2	4.76372E-11	4.68449E-11	4.60656E-11	4.53210E-11	4.40540E-11	4.29317E-11	
3	4.95668E-11	4.95320E-11	4.95819E-11	4.97370E-11	4.97761E-11	4.97647E-11	
4	1.57104E-11	1.55106E-11	1.53494E-11	1.51630E-11	1.48025E-11	1.44459E-11	
5	1.64884E-11	1.62950E-11	1.61261E-11	1.59520E-11	1.56125E-11	1.52651E-11	
6	1.66712E-11	1.65940E-11	1.65252E-11	1.64745E-11	1.63829E-11	1.62895E-11	
7	1.68379E-11	1.68429E-11	1.68591E-11	1.69239E-11	1.70000E-11	1.70755E-11	
8	1.69789E-11	1.70395E-11	1.71014E-11	1.72855E-11	1.74616E-11	1.76286E-11	
9	6.53995E-12	6.49093E-12	6.44234E-12	6.37196E-12	6.28305E-12	6.19888E-12	
10	6.70584E-12	6.65530E-12	6.60488E-12	6.53147E-12	6.43867E-12	6.35092E-12	
11	6.74392E-12	6.71755E-12	6.68702E-12	6.63779E-12	6.57822E-12	6.52351E-12	
12	6.78386E-12	6.76908E-12	6.75694E-12	6.73969E-12	6.71504E-12	6.69696E-12	
13	6.83490E-12	6.84630E-12	6.85567E-12	6.87168E-12	6.88296E-12	6.88812E-12	
14	6.88063E-12	6.91922E-12	6.94886E-12	6.98669E-12	7.03284E-12	7.07053E-12	
15	6.89868E-12	6.94356E-12	6.98475E-12	7.04072E-12	7.11248E-12	7.18250E-12	
16	0.0	0.0	0.0	0.0	0.0	0.0	
17 THROUGH 18 SAME AS ABOVE							
19	8.23372E-15	7.30207E-15	6.41157E-15	5.02883E-15	3.19705E-15	1.82348E-15	
20	8.57689E-15	7.72180E-15	6.93528E-15	5.58778E-15	3.79514E-15	2.52282E-15	
21	9.63974E-15	9.42732E-15	9.16469E-15	8.66536E-15	8.03654E-15	7.60878E-15	
22	1.12655E-14	1.18993E-14	1.25210E-14	1.34972E-14	1.47935E-14	1.59934E-14	
23	1.27943E-14	1.38171E-14	1.48985E-14	1.66067E-14	1.88089E-14	2.09150E-14	
24	4.58162E-13	4.54516E-13	4.50447E-13	4.42136E-13	4.29835E-13	4.19226E-13	
25	4.61363E-13	4.57612E-13	4.53490E-13	4.45099E-13	4.32306E-13	4.21240E-13	
26	4.61956E-13	4.59133E-13	4.56244E-13	4.49805E-13	4.40334E-13	4.31389E-13	
27	4.67375E-13	4.63005E-13	4.58287E-13	4.52959E-13	4.47339E-13	4.43420E-13	
28	4.76422E-13	4.70552E-13	4.64224E-13	4.60548E-13	4.60040E-13	4.61070E-13	
29	4.83277E-13	4.83977E-13	4.79478E-13	4.76786E-13	4.77127E-13	4.79699E-13	
30	4.82391E-13	4.89818E-13	4.95546E-13	4.97689E-13	4.99883E-13	5.01554E-13	
OZ	9						
0 M		R 1	R 2	R 3	R 4	R 5	R 6
1	3.76243E-11	3.69168E-11	3.62578E-11	3.56859E-11	3.48606E-11	3.41466E-11	
2	4.81683E-11	4.73530E-11	4.65510E-11	4.57807E-11	4.44724E-11	4.33178E-11	
3	5.00908E-11	5.00570E-11	5.01296E-11	5.02635E-11	5.02784E-11	5.02514E-11	
4	1.59295E-11	1.57366E-11	1.55334E-11	1.53643E-11	1.50353E-11	1.46422E-11	
5	1.67005E-11	1.65151E-11	1.63132E-11	1.61454E-11	1.58290E-11	1.54586E-11	
6	1.68265E-11	1.67588E-11	1.66810E-11	1.66190E-11	1.65349E-11	1.64449E-11	
7	1.69605E-11	1.69712E-11	1.70074E-11	1.70751E-11	1.71560E-11	1.72340E-11	
8	1.71238E-11	1.71849E-11	1.72825E-11	1.74698E-11	1.76222E-11	1.78123E-11	

Fig. C.2 (continued)

9	6.61027E-12	6.56135E-12	6.51256E-12	6.43941E-12	6.34240E-12	6.25081E-12	
10	6.78131E-12	6.73131E-12	6.68114E-12	6.60538E-12	6.50408E-12	6.40831E-12	
11	6.81753E-12	6.78987E-12	6.76004E-12	6.71350E-12	6.64285E-12	6.57520E-12	
12	6.85819E-12	6.84109E-12	6.82604E-12	6.80916E-12	6.77907E-12	6.74320E-12	
13	6.90701E-12	6.91040E-12	6.91379E-12	6.92344E-12	6.92918E-12	6.93182E-12	
14	6.94587E-12	6.97361E-12	6.99767E-12	7.03551E-12	7.08168E-12	7.12704E-12	
15	6.96770E-12	7.00599E-12	7.04292E-12	7.09963E-12	7.17619E-12	7.25348E-12	
16	0.0	0.0	0.0	0.0	0.0	0.0	
17 THROUGH 18 SAME AS ABOVE							
19	1.07385E-14	9.56190E-15	8.36252E-15	6.51331E-15	4.35895E-15	2.86995E-15	
20	1.12584E-14	1.02110E-14	9.00496E-15	7.27242E-15	5.22401E-15	3.75076E-15	
21	1.26241E-14	1.23824E-14	1.19526E-14	1.12858E-14	1.04530E-14	9.83281E-15	
22	1.45492E-14	1.52736E-14	1.60265E-14	1.72279E-14	1.88826E-14	2.05643E-14	
23	1.61128E-14	1.75557E-14	1.89625E-14	2.11569E-14	2.40064E-14	2.67480E-14	
24	5.71255E-13	5.64807E-13	5.58163E-13	5.48166E-13	5.36399E-13	5.26325E-13	
25	5.74543E-13	5.68109E-13	5.61382E-13	5.51132E-13	5.39148E-13	5.29041E-13	
26	5.78932E-13	5.74558E-13	5.69357E-13	5.61400E-13	5.51304E-13	5.41773E-13	
27	5.81413E-13	5.79405E-13	5.76344E-13	5.71353E-13	5.64359E-13	5.58696E-13	
28	5.85832E-13	5.88053E-13	5.87047E-13	5.83922E-13	5.81101E-13	5.80627E-13	
29	5.93214E-13	5.99577E-13	6.03322E-13	6.02006E-13	6.01525E-13	6.04179E-13	
30	5.98072E-13	6.03969E-13	6.09842E-13	6.18555E-13	6.26265E-13	6.31458E-13	
OZ	10	R 1	R 2	R 3	R 4	R 5	R 6
0 M							
1	3.81384E-11	3.73797E-11	3.66981E-11	3.60435E-11	3.51772E-11	3.44434E-11	
2	4.87102E-11	4.78702E-11	4.70471E-11	4.62496E-11	4.48981E-11	4.37093E-11	
3	5.05722E-11	5.06058E-11	5.06853E-11	5.07930E-11	5.07833E-11	5.07417E-11	
4	1.60852E-11	1.59554E-11	1.57627E-11	1.55487E-11	1.52491E-11	1.48897E-11	
5	1.68719E-11	1.67316E-11	1.65395E-11	1.63285E-11	1.60313E-11	1.56892E-11	
6	1.69306E-11	1.68904E-11	1.68286E-11	1.67511E-11	1.66757E-11	1.65948E-11	
7	1.70731E-11	1.71106E-11	1.71595E-11	1.72320E-11	1.73156E-11	1.73940E-11	
8	1.72836E-11	1.73789E-11	1.75081E-11	1.76217E-11	1.77999E-11	1.80061E-11	
9	6.67769E-12	6.62942E-12	6.58156E-12	6.51053E-12	6.41513E-12	6.31500E-12	
10	6.85256E-12	6.80359E-12	6.75484E-12	6.68227E-12	6.58401E-12	6.47875E-12	
11	6.88102E-12	6.85351E-12	6.82225E-12	6.77807E-12	6.71840E-12	6.64060E-12	
12	6.90964E-12	6.89261E-12	6.87655E-12	6.85352E-12	6.82145E-12	6.78531E-12	
13	6.94672E-12	6.95120E-12	6.95949E-12	6.96477E-12	6.97149E-12	6.97997E-12	
14	6.99209E-12	7.02090E-12	7.05475E-12	7.09898E-12	7.15605E-12	7.21432E-12	
15	7.02460E-12	7.06372E-12	7.10607E-12	7.16980E-12	7.25440E-12	7.33882E-12	
16	0.0	0.0	0.0	0.0	0.0	0.0	
17 THROUGH 18 SAME AS ABOVE							
19	1.32900E-14	1.17884E-14	1.02145E-14	8.08274E-15	5.77215E-15	4.05776E-15	
20	1.40497E-14	1.25757E-14	1.09524E-14	9.10559E-15	6.90996E-15	5.01585E-15	
21	1.57021E-14	1.53302E-14	1.47231E-14	1.39845E-14	1.30553E-14	1.22177E-14	
22	1.78919E-14	1.87035E-14	1.95426E-14	2.09326E-14	2.28175E-14	2.49290E-14	
23	1.94139E-14	2.11046E-14	2.28805E-14	2.56234E-14	2.90619E-14	3.24986E-14	
24	6.76803E-13	6.69401E-13	6.62375E-13	6.52951E-13	6.41238E-13	6.30786E-13	
25	6.80546E-13	6.73083E-13	6.65933E-13	6.56385E-13	6.44577E-13	6.33901E-13	
26	6.85510E-13	6.80623E-13	6.75322E-13	6.67716E-13	6.58007E-13	6.48896E-13	
27	6.93345E-13	6.88774E-13	6.84440E-13	6.79939E-13	6.74066E-13	6.68976E-13	
28	7.00654E-13	6.99144E-13	6.99671E-13	6.99373E-13	6.97457E-13	6.95772E-13	
29	7.06275E-13	7.08740E-13	7.14060E-13	7.20605E-13	7.23277E-13	7.24480E-13	
30	7.09462E-13	7.15679E-13	7.21712E-13	7.30779E-13	7.42624E-13	7.51876E-13	

Fig. C.2 (continued)

0AFR						
OZ	1	R 1	R 2	R 3	R 4	R 5
0 M	1	0.0	0.0	0.0	0.0	0.0
	2	1.46805E-13	1.44623E-13	1.42487E-13	1.40463E-13	1.37001E-13
	3	1.52864E-13	1.52693E-13	1.52815E-13	1.53418E-13	1.53844E-13
	4	0.0	0.0	0.0	0.0	0.0
	5	1.46805E-13	1.44623E-13	1.42487E-13	1.40463E-13	1.37001E-13
	6	1.52864E-13	1.52693E-13	1.52815E-13	1.53418E-13	1.53844E-13
	7	0.0	0.0	0.0	0.0	0.0
8 THROUGH 12 SAME AS ABOVE						
OZ	2	R 1	R 2	R 3	R 4	R 5
0 M	1	0.0	0.0	0.0	0.0	0.0
	2	5.24478E-13	5.16780E-13	5.09165E-13	5.01809E-13	4.89830E-13
	3	5.45205E-13	5.44694E-13	5.45285E-13	5.47116E-13	5.48665E-13
	4	0.0	0.0	0.0	0.0	0.0
	5	5.24478E-13	5.16780E-13	5.09165E-13	5.01809E-13	4.89830E-13
	6	5.45205E-13	5.44694E-13	5.45285E-13	5.47116E-13	5.48665E-13
	7	0.0	0.0	0.0	0.0	0.0
8 THROUGH 12 SAME AS ABOVE						
OZ	3	R 1	R 2	R 3	R 4	R 5
0 M	1	0.0	0.0	0.0	0.0	0.0
	2	2.00084E-12	1.97108E-12	1.94285E-12	1.90801E-12	1.86424E-12
	3	2.06905E-12	2.07051E-12	2.07279E-12	2.07177E-12	2.07801E-12
	4	0.0	0.0	0.0	0.0	0.0
	5	2.00084E-12	1.97108E-12	1.94285E-12	1.90801E-12	1.86424E-12
	6	2.06905E-12	2.07051E-12	2.07279E-12	2.07177E-12	2.07801E-12
	7	0.0	0.0	0.0	0.0	0.0
8 THROUGH 12 SAME AS ABOVE						
OZ	4	R 1	R 2	R 3	R 4	R 5
0 M	1	0.0	0.0	0.0	0.0	0.0
	2	8.83866E-12	8.73919E-12	8.64084E-12	8.55232E-12	8.38652E-12
	3	9.13157E-12	9.15889E-12	9.17958E-12	9.23423E-12	9.27507E-12
	4	0.0	0.0	0.0	0.0	0.0
	5	8.83866E-12	8.73919E-12	8.64084E-12	8.55232E-12	8.38652E-12
	6	9.13157E-12	9.15889E-12	9.17958E-12	9.23423E-12	9.27507E-12
	7	0.0	0.0	0.0	0.0	0.0
8 THROUGH 12 SAME AS ABOVE						
OZ	5	R 1	R 2	R 3	R 4	R 5
0 M	1	0.0	0.0	0.0	0.0	0.0
	2	1.62818E-11	1.61099E-11	1.59406E-11	1.57712E-11	1.54842E-11
	3	1.67870E-11	1.68306E-11	1.68693E-11	1.69535E-11	1.70360E-11
	4	0.0	0.0	0.0	0.0	0.0
	5	1.62818E-11	1.61099E-11	1.59406E-11	1.57712E-11	1.54842E-11
	6	1.67870E-11	1.68306E-11	1.68693E-11	1.69535E-11	1.70360E-11
	7	0.0	0.0	0.0	0.0	0.0
	8	3.46817E-14	3.43848E-14	3.41121E-14	3.37306E-14	3.31979E-14
	9	3.57675E-14	3.59502E-14	3.60993E-14	3.63268E-14	3.65853E-14
	10	0.0	0.0	0.0	0.0	0.0
	11	3.46817E-14	3.43848E-14	3.41121E-14	3.37306E-14	3.31979E-14
	12	3.57675E-14	3.59502E-14	3.60993E-14	3.63268E-14	3.65853E-14

Fig. C.2 (continued)

0Z 0 M	6	R 1	R 2	R 3	R 4	R 5	R 6
1	0.0	0.0	0.0	0.0	0.0	0.0	0.0
2	1.64648E-11	1.62890E-11	1.61152E-11	1.59421E-11	1.56487E-11	1.53799E-11	
3	1.69759E-11	1.70086E-11	1.70414E-11	1.71247E-11	1.72069E-11	1.72767E-11	
4	0.0	0.0	0.0	0.0	0.0	0.0	0.0
5	1.64648E-11	1.62890E-11	1.61152E-11	1.59421E-11	1.56486E-11	1.53799E-11	
6	1.69759E-11	1.70086E-11	1.70414E-11	1.71247E-11	1.72069E-11	1.72767E-11	
7	0.0	0.0	0.0	0.0	0.0	0.0	0.0
8	1.08674E-13	1.05832E-13	1.02656E-13	9.99861E-14	9.82884E-14	9.70308E-14	
9	1.09785E-13	1.07823E-13	1.07876E-13	1.08136E-13	1.08428E-13	1.09142E-13	
10	0.0	0.0	0.0	0.0	0.0	0.0	0.0
11	1.08674E-13	1.05832E-13	1.02656E-13	9.99861E-14	9.82884E-14	9.70308E-14	
12	1.09785E-13	1.07823E-13	1.07876E-13	1.08136E-13	1.08428E-13	1.09142E-13	
0Z 0 M	7	R 1	R 2	R 3	R 4	R 5	R 6
1	0.0	0.0	0.0	0.0	0.0	0.0	0.0
2	1.66487E-11	1.64660E-11	1.62870E-11	1.61082E-11	1.58065E-11	1.55318E-11	
3	1.71574E-11	1.71819E-11	1.72149E-11	1.72994E-11	1.73779E-11	1.74404E-11	
4	0.0	0.0	0.0	0.0	0.0	0.0	0.0
5	1.66487E-11	1.64660E-11	1.62870E-11	1.61082E-11	1.58065E-11	1.55318E-11	
6	1.71574E-11	1.71819E-11	1.72149E-11	1.72994E-11	1.73779E-11	1.74404E-11	
7	0.0	0.0	0.0	0.0	0.0	0.0	0.0
8	1.74876E-13	1.71057E-13	1.68137E-13	1.65529E-13	1.62557E-13	1.59351E-13	
9	1.81853E-13	1.79650E-13	1.78279E-13	1.77694E-13	1.77872E-13	1.78799E-13	
10	0.0	0.0	0.0	0.0	0.0	0.0	0.0
11	1.74876E-13	1.71057E-13	1.68137E-13	1.65529E-13	1.62557E-13	1.59351E-13	
12	1.81853E-13	1.79650E-13	1.78279E-13	1.77694E-13	1.77872E-13	1.78799E-13	
0Z 0 M	8	R 1	R 2	R 3	R 4	R 5	R 6
1	0.0	0.0	0.0	0.0	0.0	0.0	0.0
2	1.68385E-11	1.66461E-11	1.64611E-11	1.62762E-11	1.59636E-11	1.56764E-11	
3	1.73331E-11	1.73540E-11	1.73887E-11	1.74744E-11	1.75444E-11	1.76018E-11	
4	0.0	0.0	0.0	0.0	0.0	0.0	0.0
5	1.68385E-11	1.66461E-11	1.64611E-11	1.62762E-11	1.59636E-11	1.56764E-11	
6	1.73331E-11	1.73540E-11	1.73887E-11	1.74744E-11	1.75445E-11	1.76018E-11	
7	0.0	0.0	0.0	0.0	0.0	0.0	0.0
8	2.34820E-13	2.32818E-13	2.30688E-13	2.27021E-13	2.21970E-13	2.17698E-13	
9	2.44360E-13	2.45012E-13	2.44446E-13	2.44189E-13	2.45111E-13	2.46540E-13	
10	0.0	0.0	0.0	0.0	0.0	0.0	0.0
11	2.34820E-13	2.32818E-13	2.30688E-13	2.27021E-13	2.21970E-13	2.17698E-13	
12	2.44360E-13	2.45012E-13	2.44446E-13	2.44189E-13	2.45111E-13	2.46540E-13	
0Z 0 M	9	R 1	R 2	R 3	R 4	R 5	R 6
1	0.0	0.0	0	0.0	0.0	0.0	0.0
2	1.70255E-11	1.68316E-11	1.66355E-11	1.64456E-11	1.61272E-11	1.58248E-11	
3	1.74994E-11	1.75173E-11	1.75624E-11	1.76446E-11	1.77074E-11	1.77685E-11	
4	0.0	0.0	0.0	0.0	0.0	0.0	0.0
5	1.70255E-11	1.68316E-11	1.66355E-11	1.64456E-11	1.61272E-11	1.58248E-11	
6	1.74994E-11	1.75173E-11	1.75624E-11	1.76446E-11	1.77074E-11	1.77685E-11	
7	0.0	0.0	0.0	0.0	0.0	0.0	0.0

Fig. C.2 (continued)

		8	2.93130E-13	2.90779E-13	2.88009E-13	2.83742E-13	2.78417E-13	2.73851E-13
		9	3.01299E-13	3.04074E-13	3.05869E-13	3.07147E-13	3.08632E-13	3.10598E-13
		10	0.0	0.0	0.0	0.0	0.0	0.0
		11	2.93130E-13	2.90779E-13	2.88009E-13	2.83742E-13	2.78417E-13	2.73851E-13
		12	3.01299E-13	3.04074E-13	3.05869E-13	3.07147E-13	3.08632E-13	3.10598E-13
0Z	10							
0 M		R 1	R 2	R 3	R 4	R 5	R 6	
	1	0.0	0.0	0.0	0.0	0.0	0.0	
	2	1.71928E-11	1.70071E-11	1.68116E-11	1.66073E-11	1.62883E-11	1.59831E-11	
	3	1.76488E-11	1.76886E-11	1.77456E-11	1.78135E-11	1.78802E-11	1.79459E-11	
	4	0.0	0.0	0.0	0.0	0.0	0.0	
	5	1.71928E-11	1.70071E-11	1.68116E-11	1.66073E-11	1.62883E-11	1.59831E-11	
	6	1.76488E-11	1.76886E-11	1.77456E-11	1.78135E-11	1.78802E-11	1.79459E-11	
	7	0.0	0.0	0.0	0.0	0.0	0.0	
	8	3.48195E-13	3.45067E-13	3.41898E-13	3.37857E-13	3.32772E-13	3.28170E-13	
	9	3.58952E-13	3.60564E-13	3.62980E-13	3.66221E-13	3.69209E-13	3.71595E-13	
	10	0.0	0.0	0.0	0.0	0.0	0.0	
	11	3.48195E-13	3.45067E-13	3.41898E-13	3.37857E-13	3.32772E-13	3.28170E-13	
	12	3.58952E-13	3.60564E-13	3.62980E-13	3.66221E-13	3.69209E-13	3.71595E-13	
OFIO								
OK	1							
0 M		J 1	J 2	J 3				
	1	0.0	0.0	0.0				
	2	9.00751E-12	8.99443E-12	8.98099E-12				
	3	9.27063E-12	9.25975E-12	9.24888E-12				
	4	0.0	0.0	0.0				
	5	8.33950E-12	8.37513E-12	8.41257E-12				
	6	8.44241E-12	8.48692E-12	8.53148E-12				
	7	0.0	0.0	0.0				
	8 THROUGH 12 SAME AS ABOVE							
OK	2							
0 M		J 1	J 2	J 3				
	1	0.0	0.0	0.0				
	2	1.65713E-11	1.65465E-11	1.65211E-11				
	3	1.70270E-11	1.70050E-11	1.69830E-11				
	4	0.0	0.0	0.0				
	5	1.54020E-11	1.54643E-11	1.55293E-11				
	6	1.55815E-11	1.56584E-11	1.57354E-11				
	7	0.0	0.0	0.0				
	8	3.56073E-14	3.55257E-14	3.54482E-14				
	9	3.65572E-14	3.64883E-14	3.64195E-14				
	10	0.0	0.0	0.0				
	11	3.30814E-14	3.31697E-14	3.32816E-14				
	12	3.34002E-14	3.35433E-14	3.36867E-14				
OK	3							
0 M		J 1	J 2	J 3				
	1	0.0	0.0	0.0				
	2	1.66636E-11	1.66392E-11	1.66141E-11				
	3	1.71210E-11	1.70991E-11	1.70771E-11				
	4	0.0	0.0	0.0				
	5	1.54914E-11	1.55545E-11	1.56203E-11				
	6	1.56724E-11	1.57503E-11	1.58282E-11				
	7	0.0	0.0	0.0				
	8	7.40407E-14	7.38755E-14	7.37456E-14				
	9	7.60687E-14	7.59949E-14	7.59212E-14				
	10	0.0	0.0	0.0				
	11	6.87287E-14	6.89324E-14	6.91819E-14				
	12	6.94287E-14	6.97467E-14	7.00655E-14				

Fig. C.2 (continued)

OFJO

OK

1

0 M

	I	1	I	2	I	3	I	4	I	5
1	0.0	0.0	0.0	0.0	0.0	0.0	0.0	0.0	0.0	0.0
2	9.20777E-12	9.16808E-12	9.09390E-12	9.02061E-12	8.98217E-12					
3	9.24841E-12	9.24978E-12	9.25484E-12	9.26277E-12	9.26794E-12					
4	0.0	0.0	0.0	0.0	0.0					
5	8.40229E-12	8.39753E-12	8.38059E-12	8.35529E-12	8.33864E-12					
6	8.44205E-12	8.47744E-12	8.53762E-12	8.59025E-12	8.61496E-12					
7	0.0	0.0	0.0	0.0	0.0					

8 THROUGH 12 SAME AS ABOVE

FJO

K

1

M

	I	1	I	2	I	3	I	4	I	5
1	0.0	0.0	0.0	0.0	0.0	0.0	0.0	0.0	0.0	0.0
2	9.20777E-12	9.16808E-12	9.09390E-12	9.02061E-12	8.98217E-12					
3	9.24841E-12	9.24978E-12	9.25484E-12	9.26277E-12	9.26794E-12					
4	0.0	0.0	0.0	0.0	0.0					
5	8.40229E-12	8.39753E-12	8.38059E-12	8.35529E-12	8.33864E-12					
6	8.44205E-12	8.47744E-12	8.53762E-12	8.59025E-12	8.61496E-12					
7	0.0	0.0	0.0	0.0	0.0					

8 THROUGH 12 SAME AS ABOVE

K

2

M

	I	1	I	2	I	3	I	4	I	5
1	0.0	0.0	0.0	0.0	0.0	0.0	0.0	0.0	0.0	0.0
2	1.69114E-11	1.68427E-11	1.67149E-11	1.65890E-11	1.65230E-11					
3	1.69821E-11	1.69849E-11	1.69951E-11	1.70111E-11	1.70216E-11					
4	0.0	0.0	0.0	0.0	0.0					
5	1.55115E-11	1.55033E-11	1.54738E-11	1.54296E-11	1.54005E-11					
6	1.55809E-11	1.56428E-11	1.57482E-11	1.58406E-11	1.58842E-11					
7	0.0	0.0	0.0	0.0	0.0					
8	3.62617E-14	3.61140E-14	3.58441E-14	3.55846E-14	3.54509E-14					
9	3.64165E-14	3.64252E-14	3.64572E-14	3.65075E-14	3.65402E-14					
10	0.0	0.0	0.0	0.0	0.0					
11	3.32486E-14	3.32333E-14	3.31832E-14	3.31205E-14	3.30793E-14					
12	3.34001E-14	3.35379E-14	3.37812E-14	3.40113E-14	3.41240E-14					

K

3

M

	I	1	I	2	I	3	I	4	I	5
1	0.0	0.0	0.0	0.0	0.0	0.0	0.0	0.0	0.0	0.0
2	1.70055E-11	1.69367E-11	1.68086E-11	1.66823E-11	1.66160E-11					
3	1.70762E-11	1.70790E-11	1.70892E-11	1.71052E-11	1.71156E-11					
4	0.0	0.0	0.0	0.0	0.0					
5	1.56023E-11	1.55939E-11	1.55641E-11	1.55194E-11	1.54899E-11					
6	1.56718E-11	1.57337E-11	1.58391E-11	1.59313E-11	1.59747E-11					
7	0.0	0.0	0.0	0.0	0.0					

Fig. C.2 (continued)

8	7.55861E-14	7.52610E-14	7.46550E-14	7.40623E-14	7.37548E-14
9	7.59180E-14	7.59273E-14	7.59616E-14	7.60154E-14	7.60504E-14
10	0.0	0.0	0.0	0.0	0.0
11	6.91092E-14	6.90755E-14	6.89637E-14	6.88190E-14	6.87237E-14
12	6.94278E-14	6.97153E-14	7.02178E-14	7.06903E-14	7.09209E-14

FKO

J 1

M	I 1	I 2	I 3	I 4	I 5
1	0.0	0.0	0.0	0.0	0.0
2	1.70600E-11	1.69921E-11	1.68652E-11	1.67402E-11	1.66751E-11
3	1.71296E-11	1.71320E-11	1.71404E-11	1.71525E-11	1.71604E-11
4	0.0	0.0	0.0	0.0	0.0
5	1.56142E-11	1.56058E-11	1.55756E-11	1.55306E-11	1.55010E-11
6	1.56838E-11	1.57457E-11	1.58508E-11	1.59429E-11	1.59864E-11
7	0.0	0.0	0.0	0.0	0.0

8 THROUGH 12 SAME AS ABOVE

J 2

M	I 1	I 2	I 3	I 4	I 5
1	0.0	0.0	0.0	0.0	0.0
2	1.70376E-11	1.69693E-11	1.68419E-11	1.67164E-11	1.66507E-11
3	1.71077E-11	1.71102E-11	1.71197E-11	1.71345E-11	1.71435E-11
4	0.0	0.0	0.0	0.0	0.0
5	1.56916E-11	1.56826E-11	1.56494E-11	1.55969E-11	1.55643E-11
6	1.57617E-11	1.58236E-11	1.59271E-11	1.60150E-11	1.60570E-11
7	0.0	0.0	0.0	0.0	0.0

8 THROUGH 12 SAME AS ABOVE

J 3

M	I 1	I 2	I 3	I 4	I 5
1	0.0	0.0	0.0	0.0	0.0
2	1.70151E-11	1.69463E-11	1.68183E-11	1.66919E-11	1.66257E-11
3	1.70858E-11	1.70886E-11	1.70987E-11	1.71147E-11	1.71250E-11
4	0.0	0.0	0.0	0.0	0.0
5	1.57690E-11	1.57593E-11	1.57234E-11	1.56671E-11	1.56304E-11
6	1.58397E-11	1.59015E-11	1.60039E-11	1.60898E-11	1.61298E-11
7	0.0	0.0	0.0	0.0	0.0

8 THROUGH 12 SAME AS ABOVE

Fig. C.2 (continued)

The printed output for each group consists of the group number followed by a single line consisting of the group number (IGG), the number of directions in the DOT quadrature (MM), the dimensions of the TORT mesh (NXT,NYT,NZT), and finally the last five values of the FKO array. For group 2 only, the flux arrays AF, AFR, FIO, FJO, and FKO are printed. This output scheme reduces the amount of printed output yet still allows evaluation of values from each group.

APPENDIX D

DOTTOR OUTPUT FILE FORMAT

The DOTTOR output file is formatted according to the requirements of a TORT input file. The output file is written for 3-D geometry and contains only boundary directional data. The TORT input file format is given on the next pages.

NAME: FLXMOM

DATE: 28 JUN 84

PURPOSE: FIXED-MESH CELL MOMENT DATA, CELL SCALAR DATA,
AND/OR BOUNDARY DIRECTIONAL DATA

GEOMETRY CAN BE 1-D, 2-D, OR 3-D.

FILE MAY CONTAIN CHOICE OF CELL-AVERAGE MOMENTS
OR SCALAR DATA, BOUNDARY DIRECTIONAL DATA, OR
BOTH.

CELL MOMENTS ALONE ARE SUFFICIENT FOR A
DISTRIBUTED SOURCE OUTPUT MOMENT FILE.

BOUNDARY DATA ALONE ARE SUFFICIENT FOR A
BOUNDARY SOURCE INPUT OR OUTPUT FILE.

CELL FLUX MOMENTS AND EMERGING BOUNDARY FLUX
DATA ARE REQUIRED FOR A RESTART FILE.

MOMENT AND BOUNDARY RECORD FORMATS ARE
COMPATIBLE WITH DOT 4 FORMATS.

CELL SCALAR DATA ARE SUFFICIENT FOR A DISTRIBUTED
SOURCE INPUT FILE.

CELL SCALAR DATA ARE ALSO SUFFICIENT FOR A
RESPONSE OUTPUT FILE.

NOTES: ORDER OF GROUPS IS BY DECREASING ENERGY,
NEUTRONS, THEN PHOTONS.

I IS THE FIRST -DIMENSION INDEX.

J IS THE SECOND-DIMENSION INDEX.

K IS THE THIRD -DIMENSION INDEX.

JM=1 FOR 2-DIMENSIONAL GEOMETRY,

JM=1, KM=1 FOR 1-DIMENSIONAL GEOMETRY.

MULT = SINGLE PRECISION WORD LENGTH INDICATOR:

1 IF WORD LENGTH.GE.6 BYTES,

2 IF WORD LENGTH.LT.6 BYTES.

FILE STRUCTURE:

RECORD TYPE	PRESENT IF
FILE IDENTIFICATION	ALWAYS
FILE LABEL	ALWAYS
INTEGER PARAMETERS	ALWAYS
INTEGER ARRAYS	ALWAYS
REAL PARAMETERS & ARRAYS	ALWAYS
.....REPEAT FOR IG=1,IGM	IF NRESP.GE.0; ELSE IG=1,1
.REPEAT FOR NR=1,IABS(NRESP)	IF NRESP.NE.0; ELSE NR=1,1
.. CELL SCALAR DATA	IFMOM.GT.0 .AND. LM.EQ.0
.REPEAT ALL K=1,KM	
... CELL MOMENT DATA	IFMOM.GT.0 .AND. LM.GT.0
...END K LOOP	
.. BOUNDARY DIRECTIONAL DATA	IFBND.GT.0
.END NR LOOP	
.....END IG LOOP	

FILE IDENTIFICATION:

HNAME,(HUSE(I),I=1,2),IVERS

4*MULT = NUMBER OF WORDS

HNAME	HOLLERITH FILE NAME	- (A6)
HUSE(I)	HOLLERITH USER IDENTIFICATION	- (A6)
IVERS	FILE VERSION NUMBER	- (A6)

FILE LABEL:

DATE,USER,CHARGE,CASE,TIME,(TITL(I),I=1,12)

17*MULT = NUMBER OF WORDS

DATE	AS PROVIDED BY TIMER OPTION 4 - (A6)
USER	AS PROVIDED BY TIMER OPTION 5 - (A6)
CHARGE	AS PROVIDED BY TIMER OPTION 6 - (A6)
CASE	AS PROVIDED BY TIMER OPTION 7 - (A6)
TIME	AS PROVIDED BY TIMER OPTION 8 - (A6)
TITL(I)	TITLE PROVIDED BY USER - (A6)

INTEGER PARAMETERS:

IFMOM,IFBND,IDIM, IGM,NEUT, IM,JM,KM,LM,MM, NRESP
, (IDUM(N),N=1,14)

25 = NUMBER OF WORDS

IFMOM	1 IF MOMENT OR SCALAR RECORDS PRESENT
IFBND	1 IF BOUNDARY RECORDS PRESENT
IDIM	1/2/3 FOR 1-D, 2-D, OR 3-D
IGM	NUMBER OF ENERGY GROUPS
NEUT	LAST NEUTRON GROUP (IGM IF ALL NEUTRONS, 0 IF ALL PHOTONS)
IM	NUMBER OF I INTERVALS
JM	NUMBER OF J INTERVALS (1 IF IDIM.LT.3)
KM	NUMBER OF K INTERVALS (1 IF IDIM.EQ.1)
LM	LENGTH OF MOMENT EXPANSION; 0 FOR SCALAR DATA
MM	NUMBER OF QUADRATURE DIRECTIONS
NRESP	NUMBER OF RESPONSES; NEG IMPLIES GROUP TOTAL
IDUM(I)	ARRAY SET TO 0

INTEGER ARRAYS:**(IDUMA(I),I=1,10)****10 = NUMBER OF WORDS****IDUMA(I) ARRAY SET TO 0**

FILE REAL PARAMETERS & ARRAYS:**(X(I),I=1,IM1),(Y(J),J=1,JM1),(Z(I),I=1,KM1)
,(ENER(IG),IG=1,IGM),EMIN,ENEUT
,(DUMRL(I),I=1,8)****KM+JM+IM+3+IGM+10 = NUMBER OF WORDS**

X(I)	I-INTERVAL BOUNDARIES
Y(J)	J-INTERVAL BOUNDARIES (ABSENT IF IDIM.LT.3)
Z(K)	K-INTERVAL BOUNDARIES (ABSENT IF IDIM.EQ.1)

ENER(IG)	TOP ENERGY BOUNDARY OF GROUP IG
EMIN	BOTTOM ENERGY BOUNDARY OF GROUP IGM
ENEUT	BOTTOM ENERGY BOUNDARY OF GROUP NEUT (0 IF NEUT=0)
IM1	IM+1
JM1	JM+1
KM1	KM+1

CELL AVERAGE SCALAR DATA:

((FLIJ(I,J,K),I=1,IM),J=1,JM),K=1,KM)

IM*JM*KM = NUMBER OF WORDS

FLIJ

CELL-AVERAGE SCALAR DATA

CELL AVERAGE MOMENT DATA:

((FLUM(I,L,J),I=1,IM),L=1,LM),J=1,JM)

IM*LM*JM = NUMBER OF WORDS

REPEAT ABOVE FOR KM RECORDS

FLUM

CELL-AVERAGE MOMENT DATA

BOUNDARY DIRECTIONAL DATA:

((FIO(M,J,K),M=1,MMA),J=1,JM),K=1,KM)
, (((FJO(M,I,K),M=1,MMA),I=1,IM),K=1,KM)
, (((FKO(M,I,J),M=1,MMA),I=1,IM),J=1,JM)

MM*(JM*KM+IM*KM+IM*JM) = NUMBER OF WORDS (IDIM.EQ.3)
MM*(KM+IM) = NUMBER OF WORDS (IDIM.EQ.2)
MM = NUMBER OF WORDS (IDIM.EQ.1)

FIO I-BOUNDARY DIRECTIONAL DATA
FJO J-BOUNDARY DIRECTIONAL DATA (OMIT IF IDIF.LT.3)
FKO K-BOUNDARY DIRECTIONAL DATA (OMIT IF IDIF.EQ.1)

END

APPENDIX E

VISTA CODE DESCRIPTION

The VISTA code is an intermediate step between the DOT and DOTTOR codes. The input for the VISTA code is the scalar and angular fluxes from the DOT run and the uncollided flux from the GRTUNCL code.

VISTA first looks at the direction set and finds the directions corresponding to the uncollided flux. VISTA then reads the scalar and angular fluxes from the DOT run. The angular flux is then normalized so that the weighted sum of the angular flux equals the scalar flux. The uncollided flux, if present, is then added to the normalized directional flux. The directional flux is then written to an output file in a format suitable for use by the DOTTOR code.

INTERNAL DISTRIBUTION

- | | | | |
|--------|----------------------|--------|--|
| 1. | L. S. Abbott | 27-31. | W. A. Rhoades |
| 2. | R. G. Alsmiller, Jr. | 32. | R. W. Roussin |
| 3. | J. M. Barnes | 33. | J. C. Ryman |
| 4. | B. L. Broadhead | 34. | R. T. Santoro |
| 5. | J. A. Bucholz | 35. | C. O. Slater |
| 6. | R. L. Childs | 36. | J. S. Tang |
| 7. | S. N. Cramer | 37. | J. T. Thomas |
| 8. | H. L. Dodds, Jr. | 38-42. | J. L. Thompson |
| 9. | H. R. Dyer | 43. | D. R. Vondy |
| 10-14. | M. B. Emmett | 44. | C. C. Webster |
| 15. | W. W. Engle, Jr. | 45. | R. M. Westfall |
| 16. | W. C. Jordan | 46. | G. E. Whitesides/R. P. Leinius/
C&TD Library |
| 17. | O. W. Hermann | 47. | L. R. Williams |
| 18. | D. T. Ingersoll | 48. | A. Zucker |
| 19. | J. O. Johnson | 49. | Central Research Library |
| 20. | R. A. Lillie | 50. | ORNL-Y-12 Technical Library,
Document Reference Section |
| 21. | R. E. Maerker | 51-52. | Laboratory Records Department |
| 22. | F. C. Maienschein | 53. | Laboratory Records, ORNL RC |
| 23. | J. F. Manneschmidt | 54. | ORNL Patent Office |
| 24. | B. F. Maskewitz | | |
| 25. | J. V. Pace | | |
| 26. | J. P. Renier | | |

EXTERNAL DISTRIBUTION

- 55. J. N. Rogers, Div. 8474, Sandia National Laboratories, Livermore, CA 94550
- 56. Division of Engineering, Mathematics and Geosciences, U. S. Department of Energy, Washington, DC 20545
- 57. Office of Assistant Manager for Energy Research and Development, U. S. Department of Energy, Oak Ridge Operations, Oak Ridge, TN 37830
- 58. Dr. Paul W. Dickson, Jr., Edgerton, Germeshausen and Grier, Inc., WCBW3, P. O. Box 1625, Idaho Falls, ID 83415
- 59. Prof. Gene H. Golub, Chairman, Computer Sciences Department, Stanford University, Stanford, CA 94305
- 60. Dr. Robert M. Haralick, Vice President of Research, Machine Vision International Corp., 325 E. Eisenhower Parkway, Ann Arbor, MI 48104
- 61. Dr. Don Steiner, Institute Professor, Department of Nuclear Engineering, Rensselaer Polytechnic Institute, Troy, NY 12181
- 62-88. Technical Information Center, U. S. Department of Energy, Oak Ridge, TN 37830